TITLE:

Dynamic X-ray Diffraction Technique for Measuring Rheo-optical Properties of Crystalline Polymeric Materials

AUTHOR(S):

KAWAI, Hiromichi; ITO, Taisuke; ODA, Takashi; HIRATSUKA, Hiroaki; SUEHIRO, Shoji

CITATION:

KAWAI, Hiromichi ...[et al]. Dynamic X-ray Diffraction Technique for Measuring Rheo-optical Properties of Crystalline Polymeric Materials. Memoirs of the Faculty of Engineering, Kyoto University 1973, 35(3): 201-236

ISSUE DATE:

1973-09-29

URL:

http://hdl.handle.net/2433/280917

RIGHT:

京都大学学術情報リポジトリ
KURENAI 紅
Kyoto University Research Information Repository

Dynamic X-ray Diffraction Technique for Measuring Rheo-optical Properties of Crystalline Polymeric Materials*

By

Hiromichi KAWAI**, Taisuke ITO,*** Takashi ODA+, Hiroaki HIRATSUKA++ and Shoji SUEHIRO**

(Received March 10, 1973)

Abstract

A dynamic X-ray diffraction technique, which can follow the responses of polymer crystals (crystallization, orientation, and lattice deformation) to a mechanical excitation of sinusoidal strain induced to a bulk specimen, was described. The descriptions for such responses are qualitatively made by using a narrow sector technique, which can measure the X-ray diffraction intensity distribution at a particular phase angle of the sinusoidal strain as a function of static and dynamic strains, temperature, and angular frequency. A typical result is demonstrated in terms of the investigation of orientation-crystallization phenomena of natural rubber vulcanizates.

More quantitative descriptions can be made by using a half-circle sector technique, which can measure the in-phase and out-of phase components of the dynamic X-ray diffraction intensity distribution. From these, one can obtain the dynamic strain-induced crystallization and orientation coefficients and the dynamic response of lattice deformation of a specific crystal plane both as functions of temperature and frequency.

After a brief survey of the principle of the half-circle sector technique, frequency dependence of the dynamic strain-induced crystallization coefficients of the (002) and (200) crystal planes of natural rubber vulcanizates is demonstrated in terms of the two frequency dispersion regions around 10^{-2} and 10^{1} Hz at a room temperature. The former and latter dispersions must be correlated with the crystallization processes of the so-called

* Presented at the 2nd Discussion Conference on General Principles of Rheology, Prague, September 11–14, 1972.

** Department of Polymer Chemistry.

*** Present address: Department of Textile Dyeing, Kyoto University of Industrial Arts and Textile Fibers, Kyoto, Japan.

+ Present address: Department of Fiber and Polymer Technology, Nagoya Institute of Technology, Nagoya, Japan.

++ Present address: Ibaraki Electric Communication Laboratory, Nippon Telegraph and Telephone Public Cooperation, Tokai-mura, Ibaraki-ken, Japan.

α- and γ-filaments, respectively.

In addition, frequency and temperature dispersions of the dynamic strain-induced orientation coefficient and the dynamic response of lattice deformation of the (110) crystal plane of polyethylene are demonstrated in relation to the so-called α_1 and α_2 dispersions of dynamic mechanical modulus function of this material.

Introduction

Recent developments in the rheo-optical studies in polymer physics have revealed characteristic relaxation times of the responses of structural units in polymer solids to external mechanical excitations.[1] The basic concept for the experimental techniques used, consists of the simultaneous observation of the optical responses of the materials during deformation along with the phase of the external sinusoidal strain or another transient mechanical excitation in order to better understand the mechanical properties in terms of the responses of structural units.

Among several optical quantities which have been used for measuring the optical responses, as illustrated in Fig. 1, it must be noted that the quantities should be selected so as to correspond to the responses of definite structural units, and that the units should be distributed as widely as possible so as to cover the molecular as well as supermolecular levels. Hence, the X-ray diffraction is one of the most outstanding quantities because of a good correlation with the crystal responses of the materials, such as crystal deformation and orientation, crystallization, and crystal transition.

The application of the X-ray diffraction technique to dynamic studies is, however,

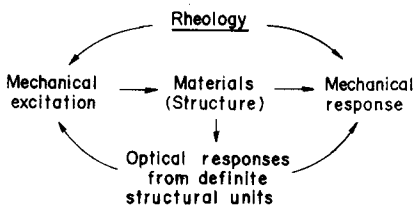

Optical responses:

Birefringence	Dichroisms (emission)
Dichroisms (absorption)	Fluorescence - dichroism
Infrared - dichroism	Laser-Raman polarization
UV-dichroism	X-ray diffraction
Dye - dichroism	Polarized light-scattering

Fig. 1. Block diagram characterizing rheo-optics in comparison with rheology and a list of several optical quantities for specific optical responses.

limited by a difficulty, namely, that the diffracted intensity obtained during a fractional phase interval of the dynamic strain is usually very weak, especially, in the frequency range of more than about 1 Hz. It obviously suffers statistical fluctuation, as well as fluctuation of intensity of the incident X-ray beam itself. This problem was overcome by application of a stroboscopic technique, in which the weak diffracted intensity was accumulated over many cycles at the same fractional phase interval of the sinusoidal strain.[2)]

Furthermore, the observation of the phase shift and the amplitude change of the diffracted intensity accompanying the forced sinusoidal strain requires great accuracy of measurement, because the diffracted X-ray intensity does not vary greatly with the strain. Also, the amplitude of the dynamic strain should be taken small in experiments of this type. The situation was much improved by a theoretical treatment of the "half-circle sector technique"[3),4)] which made possible and greatly facilitated a reliable measurement and analysis of the dynamic X-ray studies.

In this article, the dynamic X-ray diffraction techniques based on the stroboscopic technique (narrow sector technique) and the half-circle sector technique, which have been developed mostly in cooperation of the present author with Prof. R. S. Stein, Polymer Research Institute, University of Massachusetts, Amherst, Mass., U.S.A., and also some typical results of the crystal responses of polymeric materials, obtained in laboratories both in Kyoto and Amherst, are reviewed.

The dynamic X-ray diffractometer, designed and constructed by the present author, based on the stroboscopic technique, is first introduced in order to explain the "narrow sector technique". Some results obtained from the measurement of orientation-crystallization behavior of natural rubber vulcanizates by the narrow sector technique are presented. Next, the general principle of the half-circle sector technique is briefly described. Then, some results obtained by the half-circle sector technique from the measurements of the dynamic strain-induced crystallization coefficients of natural rubber vulcanizates, the dynamic strain-induced orientation coefficients of polymer crystals in a low-density polyethylene, and a dymamic lattice response of polymer crystals in a hgh-density polyethylene, are presented.

Dynamic X-ray Diffractometer Based on Stroboscopic Technique[2)]

As mentioned briefly in the introduction, the usual X-ray diffractometer equipped with an ordinary detector device, such as Geiger-Müller or scintillation counter-tube, is not quick enough in the resolution rate of the diffracted X-ray intensity and can not follow the dynamic responses, especially quick transient responses of polymer crystals. One can not help but to regard the steady state of sinusoidal responses by utilizing

some particular techniques.*

Indeed, the orientation-crystallization behavior of natural rubber vulcanizates was investigated by Singer *et al.*,[6,7] using a dynamic X-ray photographic technique in which the incident X-ray beam was chopped in synchronism with a particular phase of sinusoidal strain of the specimen; i.e., utilizing a stroboscopic technique. Quite recently, the orientation-crystallization of natural rubber vulcanizates has been again investigated by Dunning and Pennells[8] stretching continuously a running endless belt of the specimen; i.e., steadying the transient response of orintation-crystallization of rubber molecules.

Figure 2 illustrates a schematic diagram of a dynamic X-ray diffractometer constructed by the present author based on the stroboscopic technique, in which, however, the output signal from the counter-tube is chopped in contrast to the Singer's method. That is, the test specimen in ribbon shape is elongated sinusoidally by a pair of the eccentric cams which are driven by the same rate, where the static and dynamic strains of the test specimen are adjustable. This deformation device is mounted on a large circular disk, which is rotatable around its horizontal center axis. The X-ray tube and the counter-tube are made to scan in a horizontal plane simultaneously with identical Bragg angle θ, so that the X-ray diffraction intensity distribution from the test

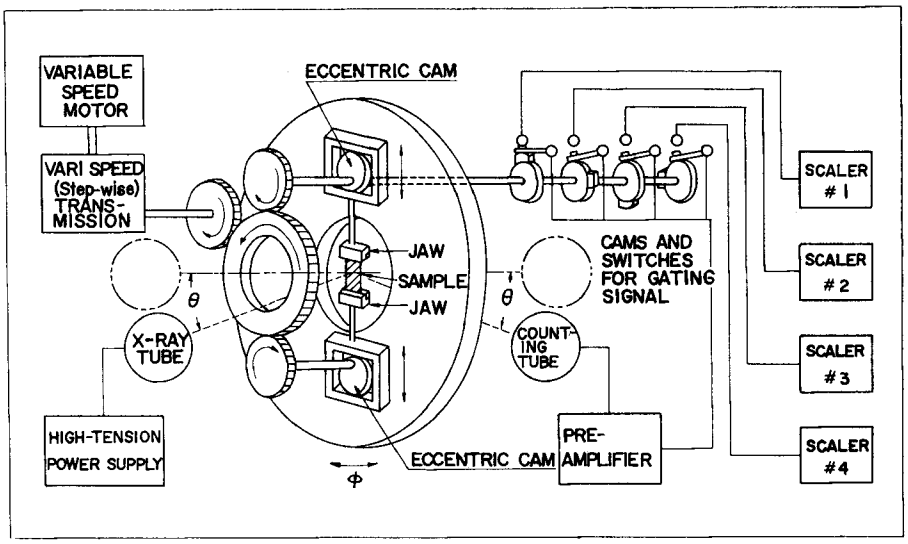

Fig. 2. Schematic diagram showing the principle of dynamic x-ray diffraction technique basing on a stroboscopic technique and the construction of the diffractometer used.

* Some attempts have been proposed for measuring the transient crystal responses by using a particular dynamic image detector composed of an image intensifier coupled to a vidicon with an out-put attached to a video recorder and conventional T.V. monitor.[5]

specimen can be measured as a function of twice the Bragg angle 2θ and the azimuthal angle ϕ even during the vibration of the specimen.

In addition, the output signal from the counter-tube is chopped by a gating device consisting of a mechanical on-off-switch for the output signal and of a nosed cam connected with the eccentric cam with a common shaft. The width of the cam nosed and its angular position with respect to the common cam shaft are adjustable. Therefore, when the gated output signal is accumulated at a given diffraction angle of 2θ and ϕ for enough cycles of the sinusoidal strain to overcome the statistical fluctuation of the incident X-ray intensity, and when this type of fixed count measurement is scanned step-wise with θ and ϕ, the X-ray diffraction intensity distribution for a given phase interval at a given phase angle can be measured as a function of some required variables, such as static and dynamic strain of the specimen, angular frequency, and temperature.

As mentioned above, this apparatus is based on the stroboscopic technique chopping the output signal, instead of the incident beam. This gives high flexibility in selection the number of the chopped phases by varying the number of the gating devices and corresponding scalers. In Fig. 2, the number of the chopped phases is taken as four shifted from each other by $\pi/2$ radians. This flexiblity has a great advantage and it is quite necessary to modify this sort of narrow sector technique to the half-circle sector technique which will be discussed later.

In practice, however, the mechanical gating device in Fig. 2 is not reliable, especially at high frequencies, because of a mechanical accelaration of the switch. The device has been modified by replacing it with a photo-electric switch, as shown in Fig. 3. Namely, a rotating disk having a narrow line slit in a radial direction and an assembly consisting of a small lightbulb on one side of the disk with a phototransistor

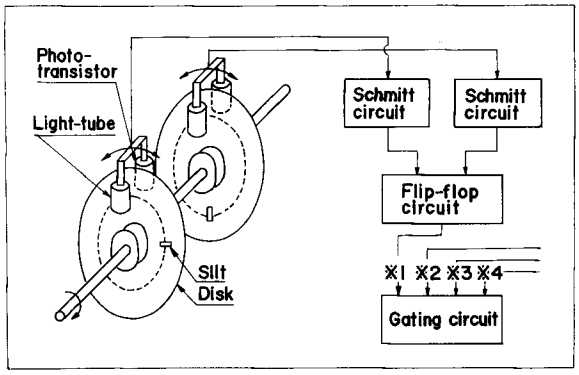

Fig. 3. Schematic diagram of a photoelectric switch set used instead of the mechanical gating device in Fig. 2. Two sets of the photoelectric switches provide gate signals for activating and deactivating each scaler.

on the other side, constitute the photoelectric switch. The assembly of the lightbulb and the phototransistor can be moved, as shown in Fig. 3, around the disk by a fine adjustable screw, even during the rotation of the disk.

Two sets of the photoelectric switches are used to produced the "on" and "off" pulse signals fed to the gating circuit through two "Schmitt" circuits and a "flip-flop" circuit for activating each scaler. The phase positions of the "on" and "off" pulses are adjustable quite flexibly with respect to the sinusoidal strain of the specimen, so that two sets of the photoelectric switches are available for the narrow sector technique for any phase interval at any phase position, and that eight sets of the switches can be used for the half-circle sector technique in which four sets of π radian phase intervals

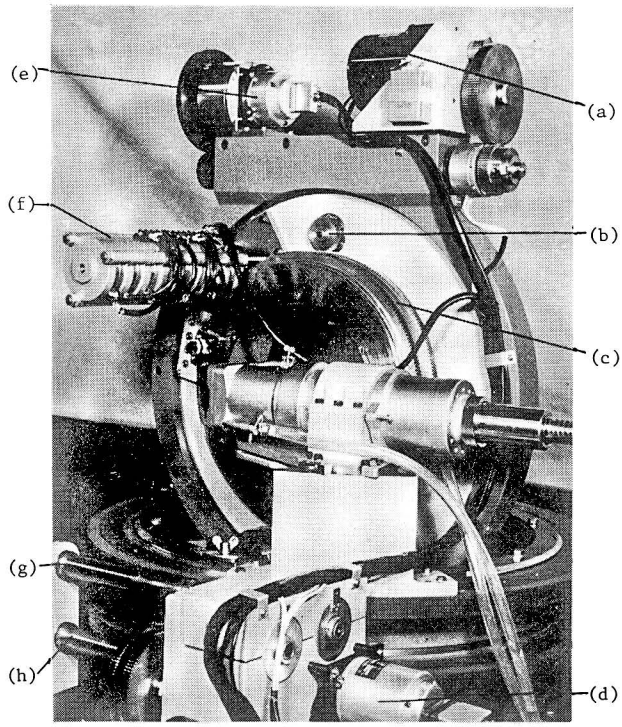

Fig. 4a. Front view of the vibration goniometer of the dynamic x-ray diffractometer constructed (equipped for transmission diffraction). (a)-driving motor for azimuthal scanning; (b)-planet gear for driving the upper eccentric cam shaft; (c)-power transmission gear wheel with two sets of teeth, one set is used for transmission of driving power from main driving shaft, and the other is common to three planet gears for two eccentric cam shafts and a shaft for photoelectric switches; (d) and (e)-shaft encoders for Bragg and azimuthal angles respectively; (f)-eight sets of photoelectric switches; (g) and (h)-driving shafts for horizontal scanning of x-ray tube and scintillation counter tube, respectively.

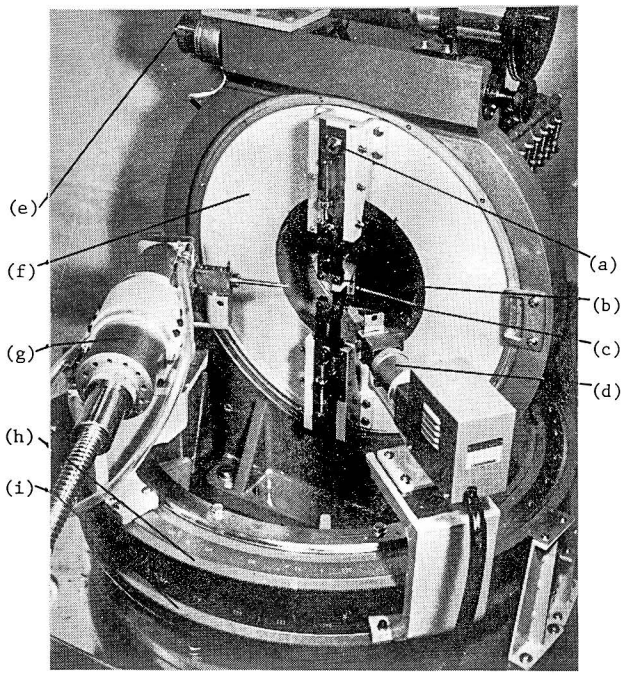

Fig. 4b. Back view of the vibration goniometer of the dynamic x-ray diffractometer constructed (equipped for reflection diffraction). (a)-upper eccentric cam inducing tensile dynamic strain of the specimen; (b)-upper jaw for holding the specimen; (c)-film specimen of crystalline polymeric materials; (d)-scintilation counter tube; (e)-driving shaft for the vertical disk; (f)-vertical disk for variation of azimuthal angle; (g)-x-ray tube; (h)-upper goniometer circle on which the x-ray tube is mounted; (i)-lower goniometer circle on which the scintilation counter tube is mounted.

must be arranged so as to shift from each other by $\pi/2$ radians. Figures 4a and 4b show front and back views of vibrational goniometer of the dynamic X-ray diffractometer constructed (equipped for transmission and reflection diffraction technique) in which eight sets of the photoelectric switches can be seen.

Narrow Sector Technique[2)]

Measurement of Orientation-Crystallization Behavior of Natural Rubber Vulcanizates by Using the Narrow Sector Technique[9)]

Figure 5 shows a variation of the degree of crystallinity with the static extension ratio at 30°C for particular specimens of sulfur-cured natural rubber (RSS No. 1) and synthetic cis-1,4-polyisoprene (Natsyn 2200) having number average molecular

weights of the network chains between crosslinks, 4150 and 3770, respectively. The second order uniaxial orientation factor* F_{20}^{c} of crystal c-axis (molecular axis) of the produced crystals is also illustrated in the figure. Although the details will be discussed in a later section of the measurement of orientation-crystallization of natural rubber vulcanizates by using the half-circle sector technique, it must be noted that the degree of crystallinity increases almost linearly with an increase of extension ratio, when the ratio becomes larger than a critical value, and that the produced crystals possess an extremely high value of the orientation factor, near unity, i.e., almost perfect orientation.

As suggested in Fig. 5, it may be interesting to investigate the dynamic orientation-crystallization behavior of these materials by using the narrow sector technique at particular phase positions as functions of angular frequency. That is, as an example for the natural rubber vulcanizate in Fig. 5, let us take the static and dynamic strains of the specimen as 300 and 50%, respectively, and observe the dynamic crystal responses

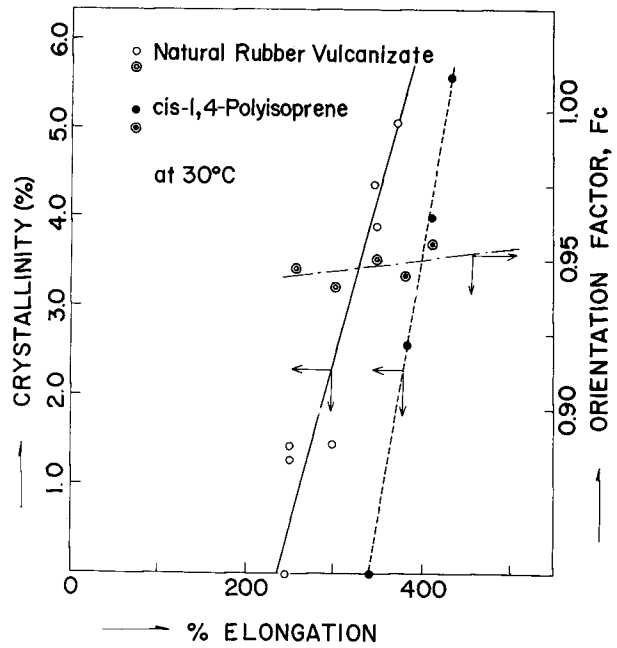

Fig. 5. Degree of crystallinity and second order uniaxial orientation factor vs. static %-elongation for particular specimens of sulfur-cured natural rubber (RSS #1) and synthetic cis-1,4-polyisoprene (Natsyn #2200).

* The second order uniaxial orientation factor F_{20}^{j} can be defined by $F_{20}^{j}=(<3\cos^2\alpha_j>-1)/2$, where α_j is the angle between the stretching direction and the jth axes of orientation units.[10]

at maximum and minimum strains, as illustrated in Fig. 6, as functions of angular frequency and temperature. The specimen must repeat crystallization and crystal-melting at the maximum and minimum strain phases respectively, unless the vibrational frequency is too high in comparison with the orientation-crystallization rate of the rubber molecules.

The dynamic X-ray diffraction intensity distribution was measured along the equatorial and meridional directions. The measurements were made at the maximum and munimum strain phases for a relatively narrow phase interval of $\pm 10°$ over a frequency range from 0.02 to 20 Hz at two different temperatures, 30 and 38°C. The necessary corrections of the observed crystalline diffraction, such as those for air-scattering, background noise, incoherent scattering, polarization, and absorption, were made.

Fresh specimens usually showed a rapid change in crystallization behavior, a sort of mechanical fatigue effect, with accumulated cycles of sinusoidal strain up to several tens of thousand of cycles, after which the reading leveled off. Therefore, every quantitative measurement of the dynamic X-ray diffraction was carried out after the accumulation of one hundred thousand cycles of dynamic strain, in order to avoid this sort of fatigue effect.

Figures 7(a) and 7(b) show the changes of the dynamic X-ray diffraction intensity distribution (normalized) along the equatorial direction at the two phase intervals, the maximum and minimum strain phases, respectively, with the number of accumulated cycles of dynamic strain at a given vibrational frequency of 2 Hz for the natural rubber

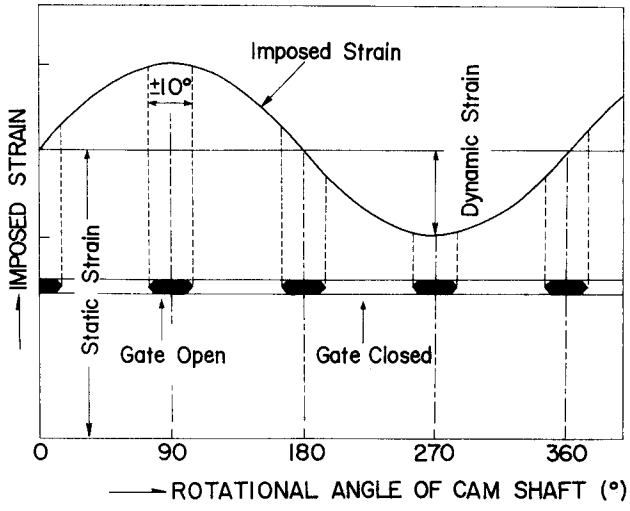

Fig. 6. Selection of phase intervals for the dynamic x-ray diffraction measurements based on the narrow sector technique.

vulcanizate. As seen in the figure, the (200) and (120) crystalline peaks appear gradually, and, in contrast, the amorphous peak degenerates. These changes seem to level off at around 1×10^3 cycles for the maximum strain phase, and at around 1×10^5 cycles for the minimum strain phase.

Figures 8(a) and 8(b) show the changes in the dynamic X-ray diffraction intensity distributions along the equatorial and meridional directions, respectively, with vibrational frequencies from 2 to 10 Hz for the natural rubber vulcanizate at 30°C. Below this frequency range, there was essentially no change in the intensity distribution. It may be noted from these figures that the crystalline diffractions from the (200), (120), and (002) planes gradually disappear with an increase in frequency; and that there exists, at least qualitatively, an anisotropy in the crystallization rate of the rubber crystal.

Figures 9(a) and 9(b) show the changes in the dynamic x-ray diffraction intensity

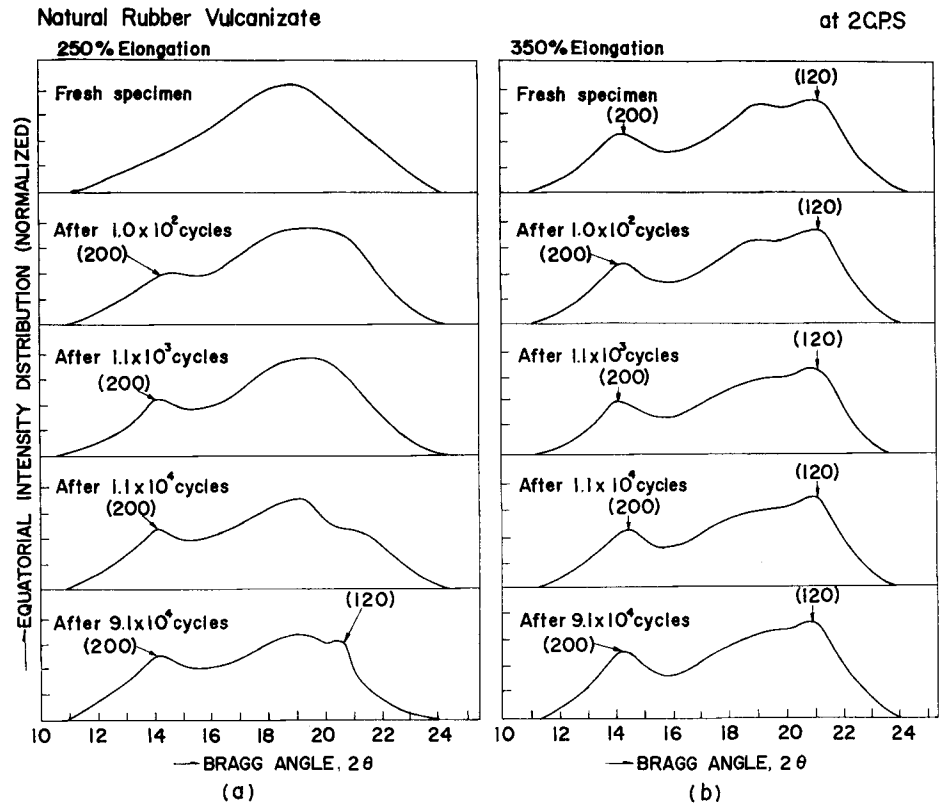

Fig. 7. Changes of dynamic x-ray diffraction intensity distributions along the equatorial direction at (a) the maximum and (b) the minimum strain phases, both with the number of accumulated cycles of dynamic strain for the natural rubber specimen under a vibrational frequency of 2 Hz at 30°C.

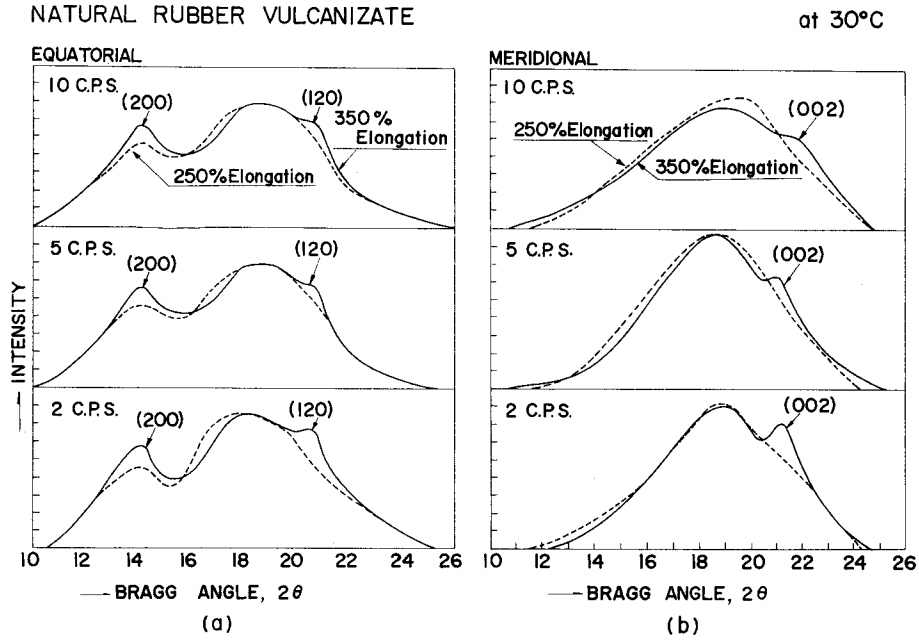

Fig. 8. Changes of dynamic x-ray diffraction intensity distributions along (a) the equatorial and (b) the meridonal directions at the maximum and minimum strain phases with vibrational frequency for the natural rubber specimen at 30°C.

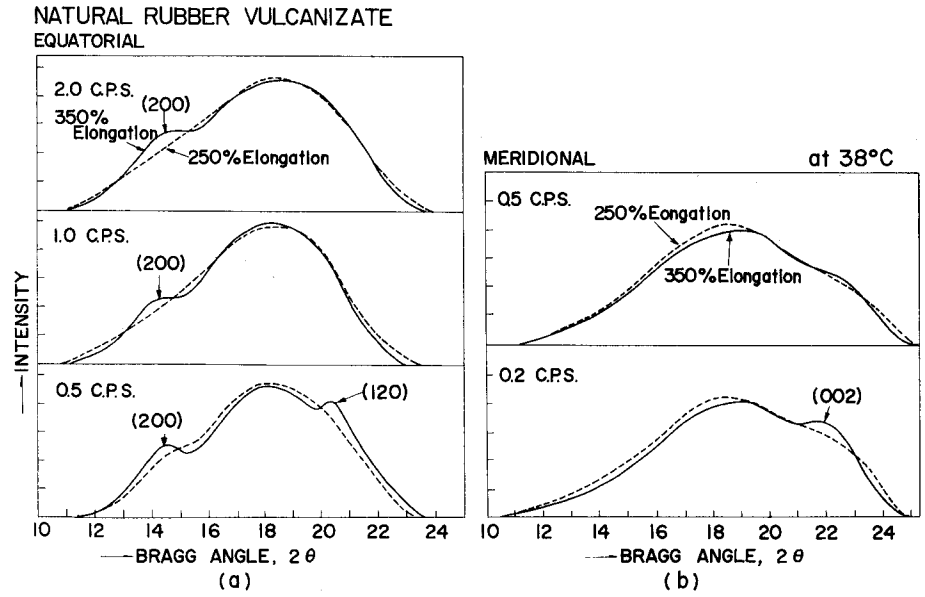

Fig. 9. Changes of dynamic x-ray diffraction intensity distributions along (a) the equatorial and (b) the meridional directions at the maximum and minimum strain phases with the vibrational frequency for the natural rubber specimen at 38°C.

distributions along the equatorial and meridional directions, respectively, with vibrational frequencies from 0.2 to 2 Hz for the natural rubber vulcanizate at a little elevated temperature of 38°C. When compared with the results at 30°C, it may be seen that the critical frequency at which the crystalline diffractions disappear becomes lower by a factor of ten, and that the anisotropy in the crystallization rate becomes more obvious. More detailed investigations and discussions are given in a later section of the measurement of orientation-crystallization of natural rubber vulcanizates by using the half-circle sector technique.

It may be concluded that the orientation-crystallization of natural rubber vulcanizates is anisotropic and becomes hard, at least in phase of dynamic strain, at around 1 to 10 Hz, depending on the crystallization temperature. This critical phenomenon must be significant in the technological view point of industrial use of the materials, if the ultimate properties of the materials are much affected by the orientation-crystallization.

Half-circle Sector Technique[4)]

General Principle[11)]

Let us assume that there are N diffraction peaks which overlap in a linear manner. Let each of the peaks be represented, as illustrated in Fig. 10, by either the Lorentzian or Gaussian function, or by any other function, such that the peaks are expressed as functions of twice the Bragg angle 2θ and of the azimuthal angle ϕ to give a symmetric functional form with respect to $2\theta_{B,j}^0$ and $\phi_{c,j}^0$, where $2\theta_{B,j}^0$ and $\phi_{c,j}^0$ are particular angles of the diffraction giving the maximum intensity $I_{m,j}^0$, i.e., the diffraction intensity distribution from the jth peak is given by

$$I_j^0(2\theta, \phi)=\chi(U_j^0)\xi(V_j^0)I_{m,j}^0 \tag{1}$$

where χ and ξ are symmetric functions with respect to $2\theta_{B,j}^0$ and $\phi_{c,j}^0$ respectively, the superscript "0" means the static situation of extension ratio $\lambda=\lambda^0$, and

$$U_j^0=(2\theta-2\theta_{B,j}^0)/\beta_j^0 \tag{2}$$

$$V_j^0=(\phi-\phi_{c,j}^0)/\gamma_j^0 \tag{3}$$

and where β_j^0 and γ_j^0 are the parameters representing the broadness of the symmetric functions, such as the half-width, if the functions are given by the Lorentzian functions.

The total diffraction intensity distribution from the N peaks can be given by

$$I^0(2\theta, \phi)=\sum_{j=1}^{N} I_j^0(2\theta, \phi) \tag{4}$$

Under the dynamic situation with sinusoidal strain given by

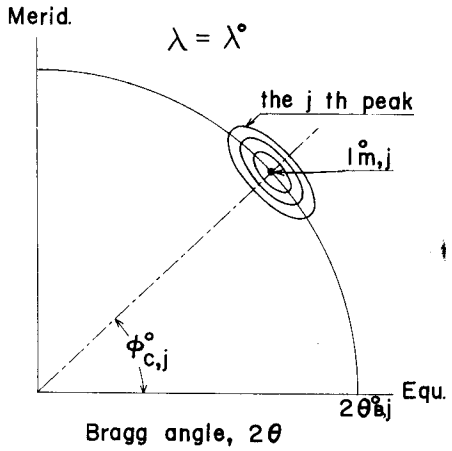

Fig. 10. Schematic diagram illustrating a x-ray diffraction intensity distribution from the jth crystal planes, having maximum intensity $I_{m,j}^0$ at twice the Bragg angle $2\theta_{B,j}^0$ and azimuthal angle $\phi_{c,j}^0$.

$$\lambda=\lambda^0+\Delta\lambda e^{i\omega t} \tag{5}$$

Let us further assume that $I_{m,j}$, $2\theta_{B,j}$, $\phi_{c,j}$, β_j, and γ_j vary also sinusoidally, as given by

$$I_{m,j}=I_{m,j}^0+\Delta I_{m,j}e^{i(\omega t-\delta_{0,j})} \tag{6}$$

$$2\theta_{B,j}=2_{B,j}^0+\Delta 2\theta_{B,j}e^{i(\omega t-\delta_{1,j})} \tag{7}$$

$$\phi_{c,j}=\phi_{c,j}^0+\Delta\phi_{c,j}e^{i(\omega t-\delta_{2,j})} \tag{8}$$

$$\beta_j=\beta_j^0+\Delta\beta_j e^{i(\omega t-\delta_{3,j})} \tag{9}$$

$$\gamma_j=\gamma_j^0+\Delta\gamma_j e^{i(\omega t-\delta_{4,j})} \tag{10}$$

where $\delta_{i,j}$ are the phase delay angles of the above dynamic quantities all with respect to the sinusoidal strain. Then, the dynamic diffraction intensity distribution from the jth crystal peak may be given by

$$I_j(2\theta,\phi)=\chi(U_j)\xi(V_j)I_{m,j} \tag{11}$$

Taking the total differential of Eq. (11), the dynamic X-ray diffraction intensity $I_j(2\theta,\phi)$ may be approximated as follows:

$$\begin{aligned}I_j(2\theta,\phi)=&a_j^0I_{m,j}^0+a_j^0\Delta I_{m,j}e^{i(\omega t-\delta_{0,j})}+b_j^0\Delta 2\theta_{B,j}e^{i(\omega t-\delta_{1,j})}\\&+c_j^0\Delta\phi_{c,j}e^{i(\omega t-\delta_{2,j})}+d_j^0\Delta\beta_j e^{i(\omega t-\delta_{3,j})}+e_j^0\Delta\gamma_j e^{i(\omega t-\delta_{4,j})}\end{aligned} \tag{12}$$

where

$$a_j^0=\chi(U_j^0)\xi(V_j^0) \tag{13}$$

$$b_j^0=I_{m,j}^0\xi(V_j^0)k_j^0 \tag{14}$$

$$c_j^0=I_{m,j}^0\chi(U_j^0)l_j^0 \tag{15}$$

$$d_j^0 = I_{m,j}{}^0 \xi(V_j^0) k_j^0 U_j^0 \tag{16}$$

$$e_j^0 = I_{m,j} \chi(U_j^0) l_j^0 V_j^0 \tag{17}$$

and where

$$k_j^0 = -(1/\beta_j^0)[\partial \chi(U_j)/\partial U_j]_{U_j = U_j^0} \tag{18}$$

$$l_j^0 = -(1/\gamma_j^0)[\partial \xi(V_j)/\partial V_j]_{V_j = V_j^0} \tag{19}$$

Consequently, the diffraction intensity at given Bragg and azimuthal angles, $I(2\theta, \phi)$ can be written as follows:

$$\begin{aligned} I(2\theta, \phi) &= \sum_{j=1}^{N} I_j(2\theta, \phi) \\ &= I^0(2\theta, \phi) + [\Delta I'(2\theta, \phi) - i\Delta I''(2\theta, \phi)] e^{i\omega t} \\ &= I^0(2\theta, \phi) + \Delta I(2\theta, \phi) e^{i(\omega t - \delta)} \end{aligned} \tag{20}$$

where

$$I^0(2\theta, \phi) = \sum_{j=1}^{N} a_j^0 I_{m,j}^0 \tag{21}$$

$$\Delta I(2\theta, \phi) = [\Delta I'(2\theta, \phi)^2 + \Delta I''(2\theta, \phi)^2]^{1/2} \tag{22}$$

$$\begin{aligned} \Delta I'(2\theta, \phi) = \sum_{j=1}^{N} [& a_j^0 \Delta I_{m,j} \cos \delta_{0,j} + b_j^0 \Delta 2\theta_{B,j} \cos \delta_{1,j} + c_j^0 \Delta \phi_{c,j} \cos \delta_{2,j} \\ & + d_j^0 \Delta \beta_j \cos \delta_{3,j} + e_j^0 \Delta \gamma_j \cos \delta_{4,j}] \end{aligned} \tag{23}$$

$$\begin{aligned} \Delta I''(2\theta, \phi) = \sum_{j=1}^{N} [& a_j^0 \Delta I_{m,j} \sin \delta_{0,j} + b_j^0 \Delta 2\theta_{B,j} \sin \delta_{1,j} + c_j^0 \Delta \phi_{c,j} \sin \delta_{2,j} \\ & + d_j^0 \Delta \beta_j \sin \delta_{3,j} + e_j^0 \Delta \gamma_j \sin \delta_{4,j}] \end{aligned} \tag{24}$$

The parameters having the superscript 0, such as a_j^0 through e_j^0, can be determined from the static measurement of x-ray diffraction intensity distribution at $\lambda = \lambda^0$, and the unknown quantities, $\Delta I_{m,j}$, $\Delta 2\theta_{B,j}$, $\Delta \phi_{c,j}$, $\Delta \beta_j$, and $\Delta \gamma_j$, and subsequently, $\delta_{0,j}$, $\delta_{1,j}$, $\delta_{2,j}$, $\delta_{3,j}$, and $\delta_{4,j}$, can be determined from the dynamic measurements of $I^0(2\theta, \phi)$, $\Delta I'(2\theta, \phi)$, and $\Delta I''(2\theta, \phi)$ by utilizing the half-circle sector technique, which will be described later, at 5 N different positions of $(2\theta, \phi)$.

Half-circle Sector Technique[3]

Before discussing the half-circle sector technique, let us take account of some correction factors, such as absorption and polarization corrections for the dynamic X-ray diffraction. During the forced periodic strain of the test specimen, the thickness of the specimen must vary in a manner which, on the assumption of incompressibility, can be calculated as follows:

$$\begin{aligned} D(t) &= D^0 - \Delta D \cos \omega t \\ &= (D_0/\sqrt{\lambda^0}) \left(1 - \frac{\Delta \lambda}{2\lambda^0} \cos \omega t\right) \end{aligned} \tag{25}$$

where D is the thickness of the specimen having D_0 at the undeformed state of $\lambda^0=1$.

If one makes the absorption and polarization corrections for the measured intensity $I(2\theta, \phi)_{exp}$, reducing the thickness always to D_0, and equates the corrected intensity with the real part of $I(2\theta, \phi)$, then the following relation will be obtained:

$$I(2\theta, \phi)=I(2\theta, \phi)_{exp}hKD_0/D(t) \tag{26}$$

where h and K are the polarization and absorption factors given by

$$h=2/(1+\cos^2 2\theta) \tag{27}$$

and

$$K=K^0Q(t)$$
$$=(1/\sec\theta)\exp(\mu D_0\sec\theta/\sqrt{\lambda^0})\exp\left[-\frac{\mu D_0\Delta\lambda}{2(\lambda^0)^{3/2}}\sec\theta\cos\omega t\right] \tag{28}$$

respectively, and where μ is the linear absorption coefficient. When one approximates $Q^{-1}(t)$ as given by

$$Q^{-1}(t)=1+[\mu D_0\Delta\lambda/2(\lambda^0)^{3/2}]\sec\theta\cos\omega t \tag{29}$$

then, Eq. (26) can be rewritten as

$$I_{exp}(t)=[1/(\lambda^0)^{1/2}hK^0][I^0-(\Delta RI^0-\Delta I')\cos\omega t+\Delta I''\sin\omega t] \tag{30}$$

where

$$\Delta R=\frac{\Delta\lambda}{2\lambda^0}[1-\mu D_0\sec\theta/(\lambda^0)^{1/2}] \tag{31}$$

Repeating n cycles of the sinusoidal strain with a given frequency of $f=\omega/2\pi$, the X-ray diffraction intensity at $(2\theta, \phi)$, accumulated for a given phase interval of the sinusoidal strain from $\alpha_1\pi$ to $\alpha_2\pi$, is given by

$$N(\alpha_1\pi\sim\alpha_2\pi)=\frac{n}{(\lambda^0)^{1/2}hK^0}[I^0(\alpha_2-\alpha_1)\pi/\omega$$
$$-\frac{\Delta RI^0-\Delta I'}{\omega}(\sin\alpha_2\pi-\sin\alpha_1\pi)-\frac{\Delta I''}{\omega}(\cos\alpha_2\pi-\cos\alpha_1\pi)] \tag{32}$$

Measuring the diffraction intensity for four particular phase intervals, $[0\sim\pi]$, $[\pi/2\sim 3\pi/2]$, $[\pi\sim 2\pi)$, and $[-\pi/2\sim\pi/2]$, as illustrated in Fig. 11 in terms of CH 1, CH 2, CH 3, and CH 4, the respective accumulated intensities can be given by

$$N_1=\frac{(n/\omega)}{(\lambda^0)^{1/2}hK^0}(\pi I^0+2\Delta I'') \tag{33}$$

$$N_2=\frac{(n/\omega)}{(\lambda^0)^{1/2}hK^0}(\pi I^0+2\Delta RI^0-2\Delta I') \tag{34}$$

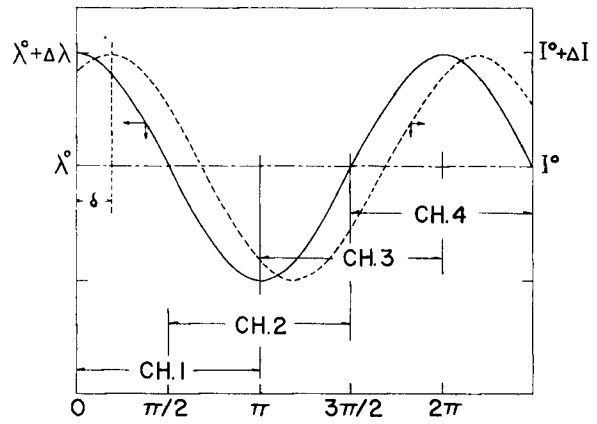

Fig. 11. Schematic diagram demonstrating the half-circle sector technique for measuring dynamic x-ray diffraction intensities for four π-radians-phase-intervals shifted from each other by $\pi/2$ radians with respect to the sinusoidal strain of test specimen.

$$N_3=\frac{(n/\omega)}{(\lambda^0)^{1/2}hK^0}(\pi I^0-2\Delta I'') \tag{35}$$

$$N_4=\frac{(n/\omega)}{(\lambda^0)^{1/2}hK^0}(\pi I^0-2\Delta RI^0+2\Delta I') \tag{36}$$

From these accumulated intensities, the necessary quantities, $I^0(2\theta, \phi)$, $\Delta I'(2\theta, \phi)$, and $\Delta I''(2\theta, \phi)$ can be determined as follows:

$$I^0(2\theta, \phi)=\frac{(\omega/2\pi)(\lambda^0)^{1/2}hK^0}{n}(N_1+N_3)$$
$$=\frac{(\omega/2\pi)(\lambda^0)^{1/2}hK^0}{n}(N_2+N_4) \tag{37}$$

$$\Delta I'(2\theta, \phi)=\frac{(\omega/2\pi)(\lambda^0)^{1/2}hK^0}{(2n/\pi)}(N_4-N_2)+\Delta RI^0 \tag{38}$$

$$\Delta I''(2\theta, \phi)=\frac{(\omega/2\pi)(\lambda^0)^{1/2}hK^0}{(2n/\pi)}(N_1-N_3) \tag{39}$$

By using the dynamic diffractometer shown in Fig. 2, equipped with four pairs of the adjustable photo-switches in Fig. 3, the accumulated intensities can be measured at 5N different diffraction angles of $(2\theta, \phi)$ for long enough cycles of n to avoid the statistical fluctuation of the incident X-ray beam.

Measurement of Dynamic Strain-induced Crystallization Coefficient of Natural Rubber Vulcanizates[12]

As already discussed briefly in the previous section of dynamic orientation-crystallization behavior of vulcanized rubbers, and will be demonstrated in detail later, the orientation-crystallization of natural rubber vulcanizates occurs in such a

particular fashion that the diffraction peaks separate from each other without any overlapping, and that the dynamic X-ray diffraction arises mostly from $\Delta I_{m,j}$ and not from $\Delta 2\theta_{B,j}$, $\Delta\phi_{c,j}$, $\Delta\beta_j$, and $\Delta\gamma_j$. Therefore, the dynamic measurements can be performed at N different position of $(2\theta_{B,j}^0, \phi_{c,j}^0)$ for the respective peaks.

Under these conditions,

$$U_j^0=0, \quad \chi(U_j^0)=1, \quad k_j^0=0$$
$$V_j^0=0, \quad \xi(V_j^0)=1, \quad l_j^0=0$$

which make b_j^0 through e_j^0 all zero and further reduce Eq. (12) to a simple one as given by

$$\begin{aligned} I_j(2\theta_{B,j}^0, \phi_{c,j}^0) &= I_{m,j}^0 + \Delta I_{m,j} e^{i(\omega t-\delta_{0,j})} \\ &= I_{m,j}^0 + (\Delta I_{m,j}' - i\Delta I_{m,j}'') e^{i\omega t} \end{aligned} \tag{40}$$

The unknown quantities, $I_{m,j}^0$, $\Delta I_{m,j}'$, and $\Delta I_{m,j}''$, and subsequently, $\delta_{0,j}=\tan^{-1}(\Delta I_{m,j}''/\Delta I_{m,j}')$ can be determined from the measurements using the half-circle sector technique at particular diffraction angles of $(2\theta_{B,j}^0, \phi_{c,j}^0)$. From the quantities, the complex dynamic strain-induced crystallization coefficient of the jth crystal plane can be defined by

$$\begin{aligned} \Delta I_{m,j}^*/\Delta\lambda|_{\lambda=\lambda^0} &= (\Delta I_{m,j}' - i\Delta I_{m,j}'')/\Delta\lambda|_{\lambda=\lambda^0} \\ &\equiv Q_j^*(i\omega) = Q_j'(\omega) - iQ_j''(\omega) \end{aligned} \tag{41}$$

The complex dynamic strain-induced crystallization coefficient Q_j^* is further a function of temperature and must be considered as one of the most basic functions for the orientation-crystallization kinetics of linear polymers. However, it must be emphasized that the coefficient Q_j^* is only related with reversible changes of crystallization which occur during the time scale of the oscillatory strain, and that the Q_j^* is quite different from irreversible changes of crystallization which follow the transient (static) strain of λ^0. In this sense, the transient strain-induced crystallization coefficient must be determined from $I_{m,j}^0$ by taking it strictly as a function of time t; i.e.,

$$I_{m,j}^0(t)/\lambda|_{\lambda=\lambda^0} \equiv Q(t) \tag{42}$$

Figure 12 shows a typical example of the X-ray diffraction intensity distribution from a highly stretched specimen of natural rubber, peroxide-cured to have a number average molecular weitht of network chain 12,800, and designated hereafter as NR-3, with an extension ratio $\lambda^0=5.5$ at a room temperature. As seen in the figure, the azimuthal distribution of the diffraction intensities from the respective crystal planes, (200), (120), (201)/($\bar{2}$01) and (002) crystal planes are highly concentrated and well-separated from each other without any overlapping. Figure 13(a) shows a typical example of the variation of the degree of crystallinity with an extension ratio at various

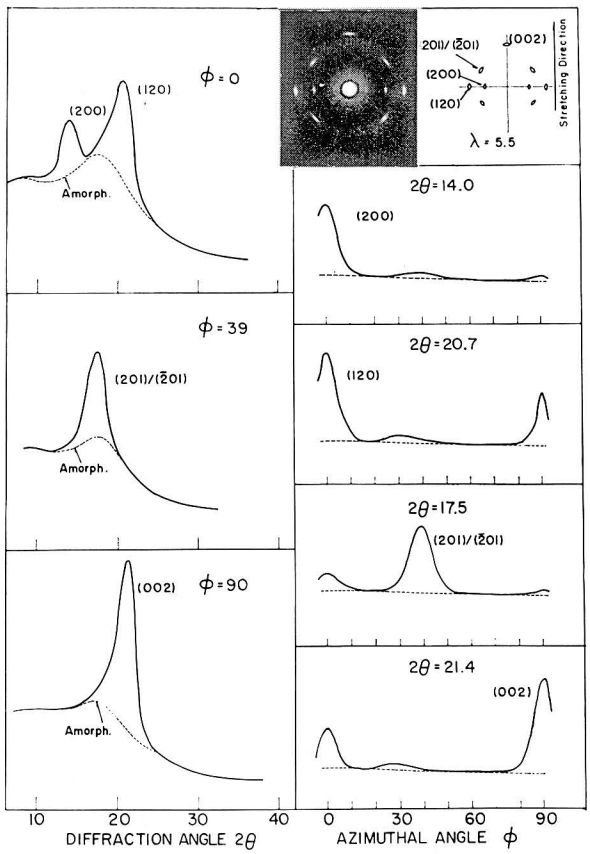

Fig. 12. Typical x-ray diffraction intensity distributions of highly stretched natural rubber vulcanizate (peroxide-cured) at toom temperature (NR-3, $\lambda^0=5.5$). The diffraction photograph attached was taken by tilting the specimen surface with respect to the incidence of x-ray beam in order to obtain the (002) diffraction.

temperatures (NR-3). As seen in the figure, the dependence of crystallinity on the extension ratio is almost linear with same slope irrespective of the stretching temperature. This suggests that the validity of an extension ratio-temperature superposition gives, as illustrated in Fig. 13(b), a slightly sigmoidal master curve reduced to a given temperature of 25°C. On the other hand, the degree of crystal orientation is hardly affected either by the extension ratio or stretching temperature, giving always an extremely high value of the second order uniaxial orientation factor of crystal c-axis, $F_{20}^{(002)}$; i.e., near perfect orientation. In other words, this extreme behavior of crystal orientation suggests that only the noncrystalline chains oriented extremely high in the stretching direction can form the crystal nuclei, probably in the fibrillar type (the so-called γ-filament by Andrews[13,14]), and on which the rubber crystals

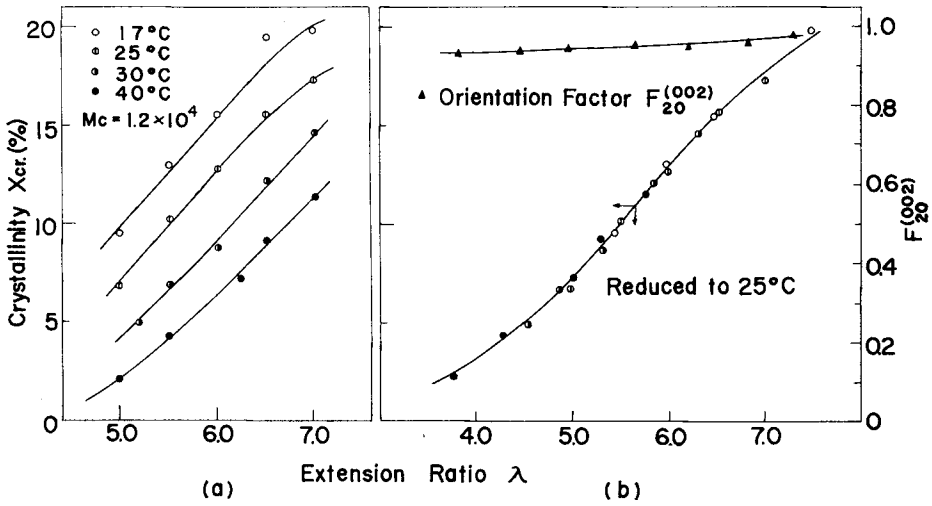

Fig. 13. Left-hand side: typical example of variation of the degree of cyrstallinity with extension ratio at various temperatures (NR-3). Right-hand side: a master curve of the degree of crystallinity against extension ratio, obtained by shifting the results in Fig. 13 (a) in the horizontal direction on the basis of extension ratio-temperature superposition hypothesis. A dependence of orientation factor on the extension ratio is also plotted.

grow epitaxially in a folded chain manner in a lateral direction (the so-called α-filament by Andrews[13,14]).

As demonstrated in Figs. 12 and 13, the diffraction intensity distributions from the respective crystal planes, such as (200), (120), and (002), separate from each other, and the intensity distributions seem to be identical and are very sharp, both irrespective of the extension ratios. Actually, as illustrated in Figs. 14 and 15 for the dynamic diffraction intensity distributions of the (200) and (002) crystal planes of the test specimen (NR-3) as a function of the azimuthal and Bragg angles, respectively, the intensity distributions are hardly affected by either the static extension ratio, dynamic frequency, or measuring temperature. Similar sharp and symmetric distributions are obtained, provided that the distributions are normalized.

These facts suggest that for the orientation-crystallization of natural rubber vulcanizates, the dynamic diffraction intensity $I_j(2\theta, \phi)$ given by Eq.(11) is mostly affected by $I_{m,j}$ and only slightly by the $\chi(U_j)\xi(V_j)$ term. In other words, $\Delta 2\theta_{B,j}$, $\Delta\phi_{c,j}$, $\Delta\beta_j$, and $\Delta\gamma_j$ in Eq.(12) are negligibly small so as to reduce Eq.(40).

Figure 16 shows variations of the dynamic strain and dynamic diffraction intensity from the (002) crystallplane, $I_{(002)}(2\theta_{B,j}^0, \phi_{c,j}^0)$, with the rotational angle of the eccentric cam shaft in Fig. 2, as obtained by using the narrow sector technique for the specimen of NR-3 at a frequency of 2.0 Hz. Although the dynamic diffraction in-

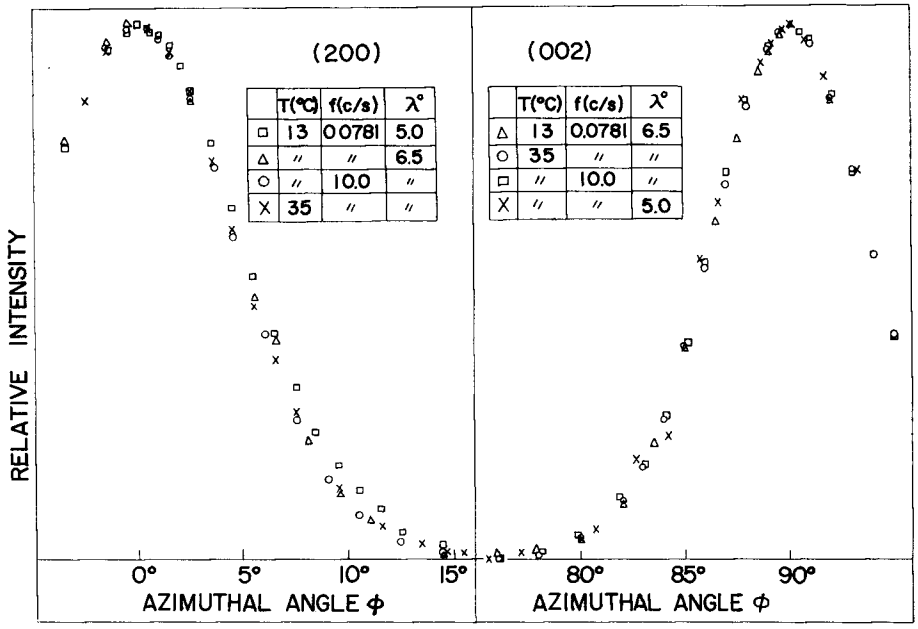

Fig. 14. Dynamic x-ray diffraction intensity distributions from (200) and (002) crystal planes with respect to azimuthal angle ϕ, obtained by using a narrow sector technique with $\Delta\lambda=0.5$, demonstrating that the distributions are very sharp and symmetric and are given by a common curve, when normalized, irerrespective of static extension ratio, temperature, and frequency.

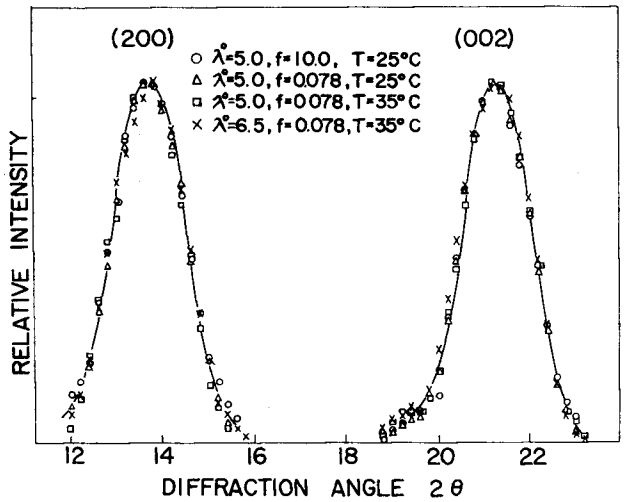

Fig. 15. Dynamic x-ray diffraction intensity distributions from (200) and (002) crystal planes with respect to twice the Bragg angle 2θ, obtained by using a narrow sector technique with $\Delta\lambda=0.5$, demonstrating that the distributions are very sharp and symmetric and are given by a common curve, when normalized, irrespective of static extension ratio, temperature, and frequency.

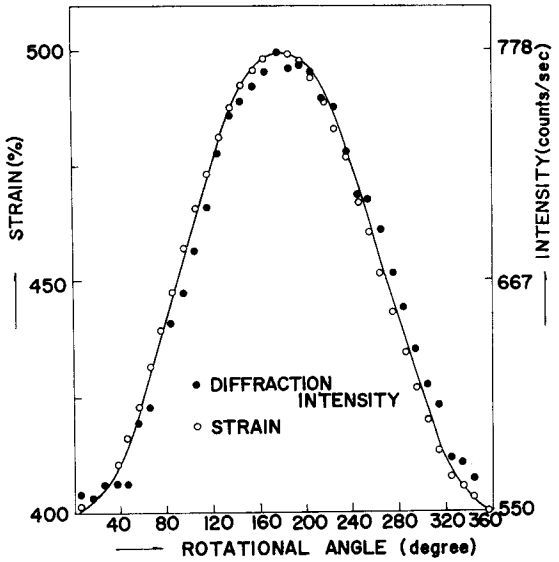

Fig. 16. Variations of the dynamic strain and dynamic x-ray diffraction intensity from (002) crystal plane, obtained by using a narrow sector technique at a given frequency of 2.0 Hz, both with rotational angle of the eccentric cam shaft in Fig. 2, demonstrating a well-proportionality between the dynamic strain and diffraction intensity.

tensity shows a slight shift to a higher rotational angle, the results demonstrate not only the sinusoidal variations of the two quantities but also a good proportion between the strain and intensity, validating, at least, the assumption of Eq.(6).

Figures 17 and 18 show the results of the measurements in terms of the frequency dependence of $\Delta I_{m,j}'$ for the test specimen of NR-3 and an additional one of about two times larger molecular weight of network chains than NR-3, keeping the dynamic strain amplitude at 0.5 and varying the measuring temperature and static extension ratio, respectively. As seen in the figures, the primary characteristic is the appearance of two frequency dispersions, one is at a relatively low frequency, around 10^{-2} Hz, and the other at a high frequency, around 10^{1} Hz. The former dispersion is most obvious for the (200) crystal plane, while the latter one is more obvious for the (002) crystal plane.

When one takes into consideration a proposal that the γ-filament must be formed almost instantaneously in association with the forced orientation of rubber molecules but that the α-filament must grow in the form of the so-called folded chain type crystal onto the side of the γ-filament, with a considerably low rate of crystallization, due to the self-diffusion of rubber molecules, then the former dispersion at the low frequency range may be assigned as arising mostly from the crystallization process of the α-

filament, while the latter one, at a higher frequency range, may be attributed to the crystallization process of the γ-filament.

In addition to the above characteristic, it is also noted that the value of $\tan\delta_{0,j}$, although relatively small, around 0.02, is definitely positive.* This is illustrated in Fig. 17 for just one example in order to avoid increasing the complexity of the figure. In other words, the dynamic orientation-crystallization of natural rubber vulcanizates occurs in advance of the dynamic strain of the specimen; it probably is in plase with the dynamic stress of the specimen.

Figure 17 demonstrates the effect of temperature upon the frequency dispersion of $\Delta I_{m,j}'$ for the additional specimen, NR-1, keeping the static strain at a relatively high value of 6.5 and the dynamic strain amplitude at 0.5. As seen in the figure, the magnitude of $\Delta I_{m,(002)}'$ is larger than that of $\Delta I_{m,(200)}'$ at relatively low temperatures. However, with increasing temperature, $\Delta I_{m,(002)}'$ decreases more rapidly and probably becomes smaller than $\Delta I_{m,(200)}'$ at temperatures higher than 40°C. Although the frequency dispersions on the low and high frequency sides, which are obvious for the (200) and (002) crystal planes, respectively, become less obvious with increasing temperature, the disperion at the low frequency side seems to shift to higher

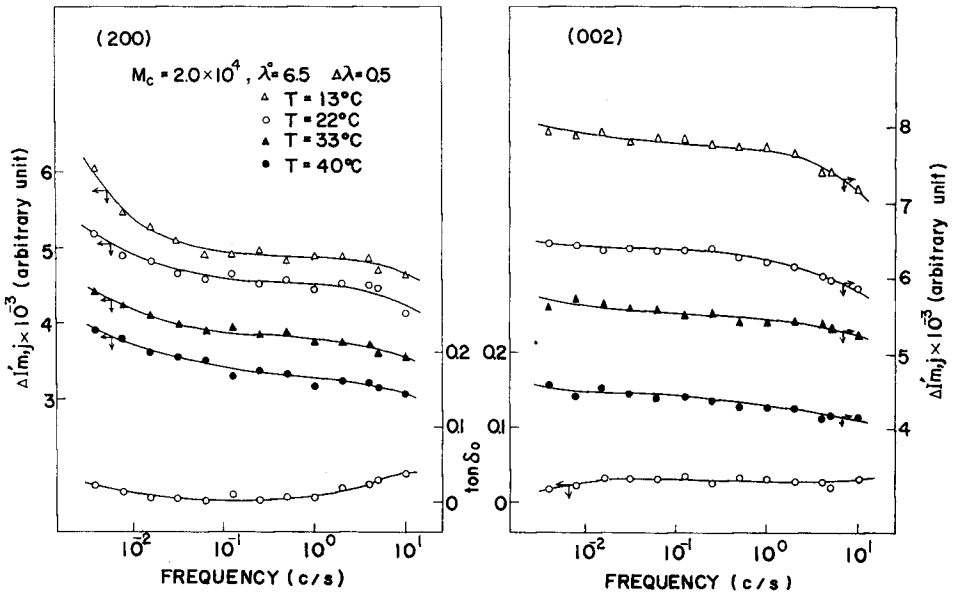

Fig. 17. Effect of measuring temperature upon the frequency dispersions of $\Delta I_{m,j}'$ for a natural rubber vulcanizate (NR-1) with keeping the static extension ratio at relatively high value of 6.5 and the dynamic strain amplitude at 0.5.

* As seen in Eq. (6), $I_{m,j}$ is defined as being behind the dynamic strain λ, but the observed value of $\delta_{o,j}$ is always negative so that $\tan\delta_{o,j}$ must be positive.

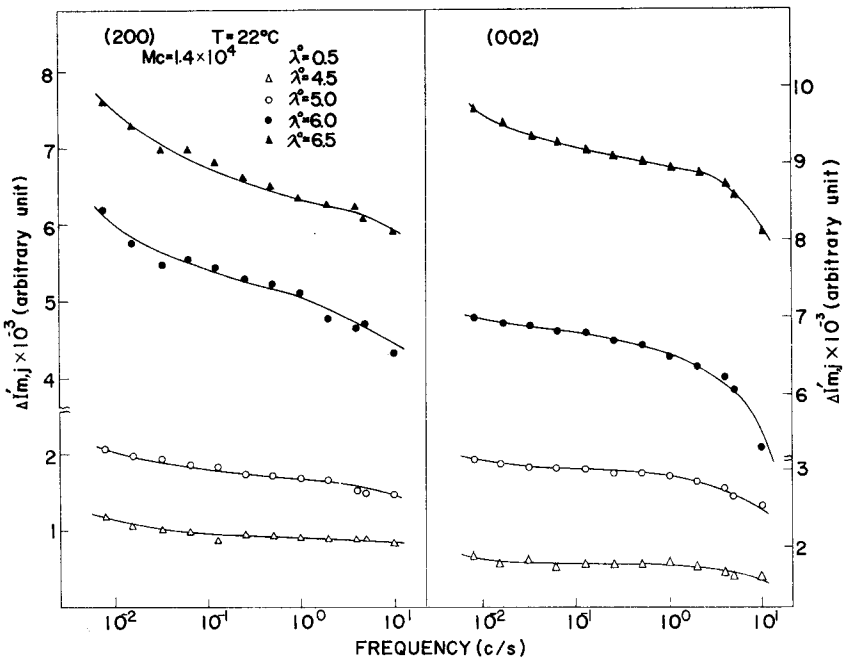

Fig. 18. Effect of static extension ratio upon the frequency dispersions of $\Delta I_{m,j}'$ for a natural rubber vulcanizate (NR-3) with keeping the measuring temperatuer at 22°C and the dynamic strain amplitude at 0.5.

frequencies with increasing temperature, while that at the high frequency side seems not to shift at all.

Figure 18 shows the effect of static strain upon the frequency dispersions of $\Delta I_{m,j}'$ for the specimen of NR-3, keeping the measuring temperature at 22°C and dynamic strain amplitude at 0.5. As seen in the figure, the effect of a decreasing static strain on the frequency dispersions seems to be similar, at least qualitatively, with that of an increasing temperature; that is, the lower the static strain, the less obvious the dispersions, likewise the magnitudes of $\Delta I_{m,j}'$ decreased when the temperature increased. The shift of the low frequency dispersion to higher frequencies (which is also observed in Fig. 18 to some extent for $\Delta I_{m,(200)}'$), may be interpreted in terms of the same factors, i.e., the increasing mobility of self-diffusion of rubber molecules to form the α-filament with decreasing static strain and increasing temperature.

Measurement of Dynamic Strain-induced Orientation Coefficient of Polymer Crystals in A Low-density Polyethylene[3,15]

Assuming that the dynamic orientation of polymer crystals is associated only with $I_{m,j}\xi(V_j)$, but not with $\chi(U_j)$ in Eq.(11); i.e., only with $\Delta I_{m,j}$, $\Delta\phi_{c,j}$, $\Delta\gamma_j$, but not

with $\Delta 2\theta_{B,j}$ and $\Delta\beta_j$, which may meet with the deformation of semicrystalline polymers (relatively low degree of crystallinity) with a relatively small dynamic strain, then the dynamic measurements can be performed at particular diffraction angles of ($2\theta_{B,j}^0$, ϕ) for the respective diffraction peaks.

Under these conditions,

$$U_j^0=0, \quad \chi(U_j^0)=1, \quad \text{and} \quad k_j^0=0$$

then, Eq.(12) can be written as

$$I_j(2\theta_{B,j}^0, \phi)=I_j^0(2\theta_{B,j}^0, \phi) + [\Delta I_j'(2\theta_{B,j}^0, \phi)-i\Delta I_j''(2\theta_{B,j}^0, \phi)]e^{i\omega t} \tag{43}$$

where

$$I_j^0(2\theta_{B,j}^0, \phi)=a_j^0 I_{m,j}^0=\xi(V_j^0)I_{m,j}^0 \tag{44}$$

$$\Delta I_j'(2\theta_{B,j}^0, \phi)=a_j^0\Delta I_{m,j}\cos\delta_{0,j}+c_j^0\Delta\phi_{c,j}\cos\delta_{2,j}+e_j^0\Delta\gamma_j\cos\delta_{4,j} \tag{45}$$

$$\Delta I_j''(2\theta_{B,j}^0, \phi)=a_j^0\Delta I_{m,j}\sin\delta_{0,j}+c_j^0\Delta\phi_{c,j}\sin\delta_{2,j}+e_j^0\Delta\gamma_j\sin\delta_{4,j} \tag{46}$$

The unknown quantities, $\Delta I_{m,j}$, $\Delta\phi_{c,j}$, and $\Delta\gamma_j$, and subsequently, $\delta_{0,j}$, $\delta_{2,j}$, and $\delta_{4,j}$, can be determined from the dynamic measurements of $I^0{}_j(2\theta_{B,j}^0, \phi)$, $\Delta I_j'(2\theta_{B,j}^0, \phi)$ and $\Delta I_j''(2\theta_{B,j}^0, \phi)$ by using the half-circle sector technique at 3 N different positions of $(2\theta_{B,j}^0, \phi)$; i.e., $(2\theta_{B,j}^0, \phi_{c,j}^0)$, $(2\theta_{B,j}^0, \phi_{1,j}^0)$, and $(2\theta_{B,j}^0, \phi_{2,j}^0)$.

Defining the second order uniaxial orientation factor of reciprocal lattice vector of the jth crystal plane, as given in the foot note in page 8, i.e.,

$$F_{20}{}^j=(3\langle\cos^2\alpha_j\rangle-1)/2 \tag{47}$$

where

$$\langle\cos^2\alpha_j\rangle=\int_0^{\pi/2} I_{m,j}^0(\phi)\sin^2\phi\cos\phi\, d\phi \Big/ \int_0^{\pi/2} I_{m,j}^0(\phi)\cos\phi\, d\phi \tag{48}$$

and further defining $S_{j,i}^0$, $\Delta S_{j,i}'$, $\Delta S_{j,i}''$ as follows;

$$S_{j,1}^0=\int_0^{\pi/2} I_{m,j}^0(\phi)\sin^2\phi\cos\phi\, d\phi \tag{49}$$

$$S_{j,2}^0=\int_0^{\pi/2} I_{m,j}^0(\phi)\cos\phi\, d\phi \tag{50}$$

$$\Delta S_{j,1}'=\int_0^{\pi/2} \Delta I_j'(\phi)\sin^2\phi\cos\phi\, d\phi \tag{51}$$

$$\Delta S_{j,2}'=\int_0^{\pi/2} \Delta I_j'(\phi)\cos\phi\, d\phi \tag{52}$$

$$\Delta S_{j,1}''=\int_0^{\pi/2} \Delta I_j''(\phi)\sin^2\phi\cos\phi\, d\phi \tag{53}$$

$$\Delta S_{j,2}''=\int_0^{\pi/2} \Delta I_j''(\phi)\cos\phi\, d\phi \tag{54}$$

then, the orientation factor can be written as

$$F_{20}{}^{j}=F_{20}{}^{j0}+\Delta F_{20}{}^{j}e^{i(\omega t-\sigma)}$$
$$=F_{20}{}^{j0}+(\Delta F_{20}{}^{j'}-i\Delta F_{20}{}^{j''})e^{i\omega t} \tag{55}$$

where

$$F_{20}{}^{j0}=[3(S_{j,1}{}^{0}/S_{j,2}{}^{0})-1]/2 \tag{56}$$
$$\Delta F_{20}{}^{j'}=(S_{j,1}{}^{0}/S_{j,2}{}^{0})[(\Delta S_{j,1}{}'/S_{j,1}{}^{0})-(\Delta S_{j,2}{}'/S_{j,2}{}^{0})] \tag{57}$$
$$\Delta F_{20}{}^{j''}=(S_{j,1}{}^{0}/S_{j,2}{}^{0})[(\Delta S_{j,1}{}''/S_{j,1}{}^{0})-(\Delta S_{j,2}{}''/S_{j,2}{}^{0})] \tag{58}$$

From the complex dynamic orientation factor $\Delta F_{20j}{}^{*}$, the complex dynamic strain-induced orientation coefficient of the jth crystal plane $C_j{}^{*}(i\omega)$ can be defined by

$$\Delta F_{20}{}^{j*}/\Delta\lambda|_{\lambda=\lambda^0}=(\Delta F_{20}{}^{j'}-i\Delta F_{20}{}^{j''})/\Delta\lambda|_{\lambda=\lambda^0}$$
$$\equiv C_j{}^{*}(i\omega)=C_j{}'(\omega)-iC_j{}''(\omega) \tag{59}$$

Figures 19 and 20 show the master curves of frequency dependence of real part of the complex dynamic strain-induced orientation coefficient $C_j{}^{*}(\omega c_T)$ for two kinds of test specimens of a low density polyethylene, "Q" and "H", respectively. The Q

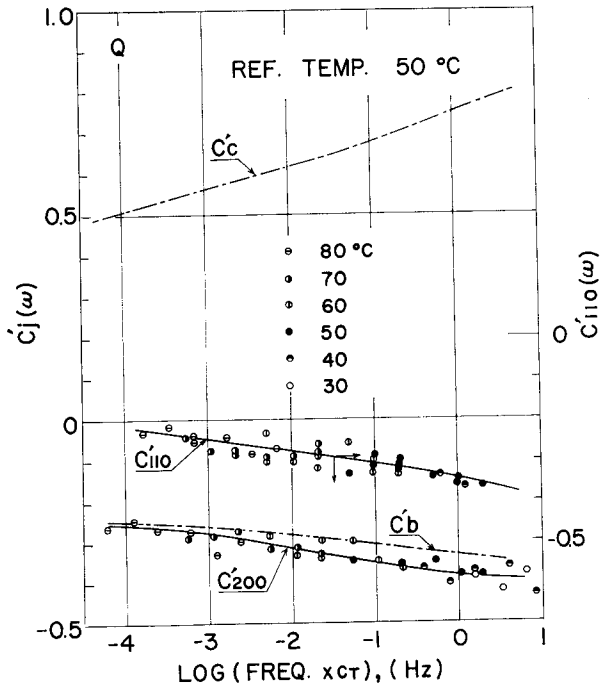

Fig. 19. Master curves of frequency dependence of real part of the complex dynamic strain-induced orientation coefficient $C_j{}^{*}(\omega c_T)$ for a quenched low density polyethylene. (after Stein et al.[15]).

specimen was quenched from melt at 155°C to have a bulk density of 0.914 and a degree of crystallinity of 45.8%, while the H specimen was obtained by annealing the Q specimen at 90°C for two hours to provide a bulk density of 0.921 and a degree of crystallinity of 50.5%. The master curves were composed of the data of $C_j'(\omega)$ at various temperatures on the basis of the time-temperature superposition hypothesis[16] and reduced to T_0, a given reference temperature of 50°C, in association with the so-called shift factor $c_T(T, T_0)$.[16] In every figure, the results of crystal c- and b-axes were calculated from the experimental results of reciprocal lattice vectors of (110) and (200) crystal planes, i.e., $C_{(110)}'(\omega)$ and $C_{(200)}'(\omega)$, by using Wilchinsky's relation[18] and an orthogonal relation between the crystal a-, b-, and c-axes, respectively.

As seen in the Figures 19 and 20, dynamic orientation behavior of each crystal axis is much different in the two specimens, Q and H. The reason for this is definitely because of the differences in crystalline and supermolecular crystalline (spherulitic) structures in the specimens; i.e., differences in the size and perfection of the crystalline lamellae, the smoothness of their surfaces, the inter-lamellar spacing, and the viscosity of the inter-lamellar material. With increasing annealing, the lamellae get thicker and more perfect, and closer together so that inter- and intra-lamellar crystalline responses become more difficult and take more time. In this sense, the results in Fig. 19 for Q specimen must be understood, at least qualitatively, as results expected for the H specimen at lower frequencies than those covered in Fig. 20.

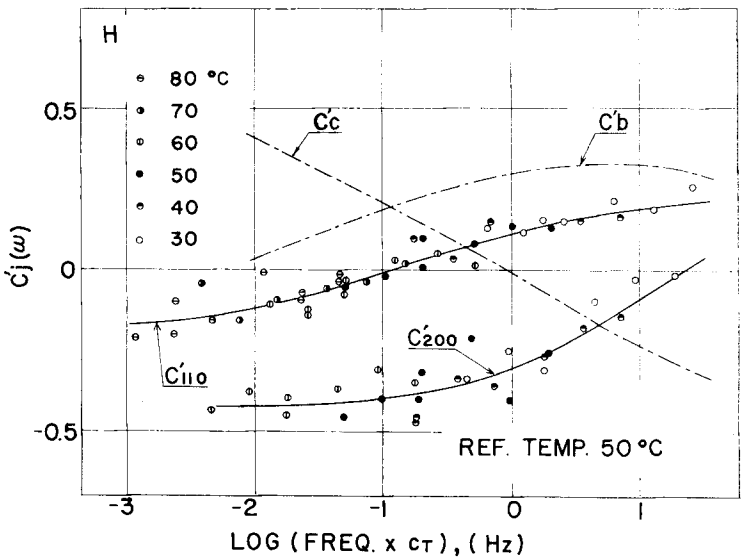

Fig. 20. Master curves of frequency dependence of real part of the complex dynamic strain-induced orientation coefficient $C_j^*(\omega c_T)$ for an annealed low density polyethylene. (after Stein et al.[15]).

For the quenched specimen in Fig. 19, values of C_a' and C_b' are negative and quite close to each other, indicating no preferential orientation of the a- or b-axis. The positive C_c' indicates an orientation mechanism in which the c-axis aligns parallel to the stretching direction, as might be expected for example from the floating rod model of Kratky.[19] There should be a maximum in C_c' and a minimum in C_a' and C_b', all at higher frequencies than the frequency range covered, as expected from the continuity to Fig. 20 mentioned above. For the H specimen in Fig. 20, on the other hand, C_a' and C_b' are quite different from each other. While C_a' is negative at all frequencies covered, C_b' becomes positive at higher frequencies. C_c' becomes negative at higher frequencies in contrast to the behavior of the Q specimen for which C_c' is always positive and increases with an increase of frequency.

The dynamic behavior of the H specimen, especially at higher frequencies, must be interpreted in terms of a spherulite deformation mechanism. It has been pointed out that the b-axis is unique in spherulitic polyethylene in that it is directed along the spherulite radius while the a- and c-axes are perpendicular to the radius.[20] Also it has been shown that the deformation of the sample is accompanied by the deformation of spherulite i.e., alignments of crystal lamellae, growing radially within the spherulite, in the streching direction.[21,22] High speed[23,24] and dynamic light scattering studies[25,26] have shown that this spherulite deformation is very fast, occuring in times comparable with that for specimen deformation. Consequently, the behavior at higher frequencies can be explained in terms of dynamic orientation of crystal lamellae within the spherulite, giving positive orientation of the crystal b-axis (lamellar axis) and almost identical negative orientations of crystal a- and c-axes.

As suggested again from the dynamic light scattering studies,[26] two additional processes must be considered at lower frequencies in Fig. 20. One is the lamellar twisting process involving a rotation about the b-axis, bringing the c-axis into the plane containing the lamellar axis and stretching direction. The other would be a rotation about the a-axis where the c-axis rotates toward the stretching direction and b-axis rotates away from the spherulite radius. The former process would predominate in the equatorial part of the spherulite while the latter process predominates in the polar part of the spherulite, as theoretically demonstrated by Stein *et al.*[27,28] and also by Kawai *et al.*[29–31]. These kinds of crystal reorientations within the lamellae lags the lamellar orientation (spherulite deformation) and results in the positive orientation of the crystal c-axis and negative orientations of crystal b- as well as a-axes. The processes of crystal motions associated with tilting and twisting of the c-axis within the lamellae, i.e., the dissipation process involving inter-lamellae motion or else that of intra-lamellar motion (relative motion of mosaic blocks constituting the lamellae), represents a viscoelastic loss reflected in the mechanical tanδ, assigned as the so-called

α_1 dispersion.

The existence of a maximum in the positive orientation of c-axis and of a minimum in the negative orientations of a- and b-axes at low frequencies than the range covered in Fig. 20 and, consequently, the behavior shown in Fig. 19 for the Q specimen, can not be explained in terms of the mechanisms suggested above. A second process must be introduced which leads to decreasing orientation changes with decreasing frequency (increasing temperature) in order to realize the maximum or the minimum. This process may be a sort of premelting or disordering of crystals in which internal mobility develops.[29,32] This occurs at a temperature close to that at which there is an increase in the rate of expansion of the crystal a-axis[33], and where a dielectric α loss process is observed[34,35] which is related to the onset of a rotation of polar groups within crystals.

In this region there is a significant drop in modulus so that the dropoffs in C_c' in positive sign and in C_a' and C_b' in negative sign can be considered the result of a decrease in stress which is the driving force of crystal orientation changes. The tendency for this process to occur depends upon the size and perfection of the crystals. Mobility of chains is less within larger and more perfect crystals. The more quenched specimens presumably possess spherulites within which crystals are relatively free to change

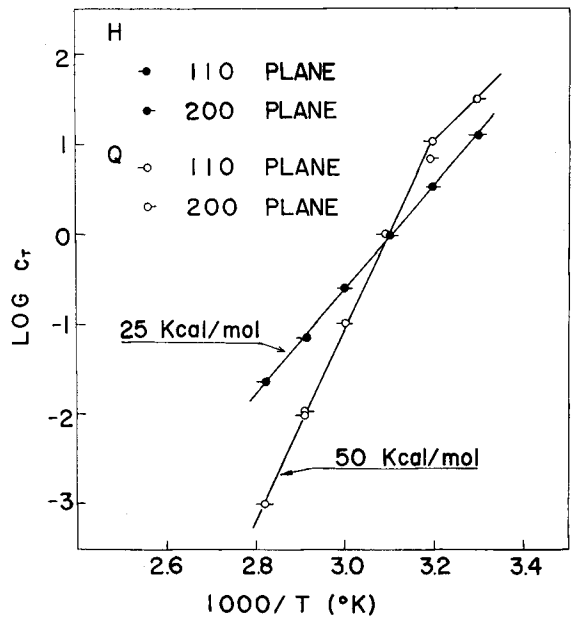

Fig. 21. Temperature dependence of the shift factor c_T in terms of its logarithmic plot against reciprocal of absolute temperature for the quenched and annealed low density polyethylenes, Q and H. (after Stein et al.[15]).

their orientation without constraints imposed by their location within the spherulites. Since the difference in orientation behavior in the a- and b-axes result from their unique orientations of the axes within the spherulites, this difference vanishes in the more highly quenched specimens.

Figure 21 shows the temperature dependence of the shift factor c_T in terms of its logarithmic plot against a reciprocal of absolute temperature. As seen in the figure, the results of the (110) and (200) crystal planes for each specimen of Q and H agree well, giving a single straight line for the H specimen with activation energy of about 25 Kcal/mole, and also a single straight line bent at relatively low temperature for the Q specimen with activation energy of 50 Kcal/mole. The difference in activation energy may reflect the difference in the primary relaxation processes for the two specimens. The higher value for the Q specimen is believed to be associated with the α_2 intracrystalline premelting or disordering type of processes. The lower value for the H specimen is believed to be associated with the α_1 mosaic rotation and lamellar twist processess, which will be discussed later in relation to the α_2 and α_1 mechanical dispersions of the materials.

Measurement of Dynamic Lattice Responses of Polymer Crystals in A High-density Polyethylene[36]

In the previous section, the dynamic orientation behavior of polymer crystals against sinusoidal mechanical excitation was discussed on the basis of neglecting $\Delta 2\theta_{B,j}$ and $\Delta\beta_j$, which may meet with a low-density polyethylene, a rather soft crystalline material with low degree of crystallinity. In this section, let us treat the dynamic response of polymer crystal more rigorously, just neglecting $\Delta\beta_j$, and investigate the dynamic lattice response of a high-density polyethylene mainly in terms of $\Delta 2\theta_{B,j}$.

For the measurement of dynamic lattice response, the peak shift in a direction of a given azimuthal angle, $\phi_{k,j}^0$ must be taken into account, and the measuring position can be fixed at $(2\theta, \phi_{k,j}^0)$. Under these conditions, V_j^0, $\xi(V_j^0)$ and l_j^0 must be constant, and Eq.(12) can be reduced to

$$I_j(2\theta)=I_j^0(2\theta)+[\Delta I_j'(2\theta)-i\Delta I_j''(2\theta)]e^{i\omega t} \tag{60}$$

where

$$I_j^0(2\theta)=a_{j,k}^0 I_{m,j}^0=\chi(U_j^0)I_{k,j}^0 \tag{61}$$

$$\Delta I_j'(2\theta)=a_{j,k}^0\Delta I_{m,j}\cos\delta_{0,j}+b_{j,k}^0\Delta 2\theta_{B,j}\cos\delta_{1,j} +c_{j,k}^0\Delta\phi_{c,j}\cos\delta_{2,j}+d_{j,k}^0\Delta\beta_j\cos\delta_{3,j}+e_{j,k}^0\Delta\gamma_j\cos\delta_{4,j} \tag{62}$$

$$\Delta I_j''(2\theta)=a_{j,k}^0\Delta I_{m,j}\sin\delta_{0,j}+b_{j,k}^0\Delta 2\theta_{B,j}\sin\delta_{1,j} +c_{j,k}^0\Delta\phi_{c,j}\sin\delta_{2,j}+d_{j,k}^0\Delta\beta_j\sin\delta_{3,j}+e_{j,k}^0\Delta\gamma_j\sin\delta_{4,j} \tag{63}$$

Assuming that the change of β_j is negligibly small; i.e. $\Delta\beta_j\cong 0$, then Eqs. (62)

and (63) can be approximated to give

$$\Delta I_j^*(2\theta)=M\Delta I_{k,j}^*+N\Delta 2\theta_{B,j}^* \tag{64}$$

where

$$M=I_j^0/I_{k,j}^0 \tag{65}$$

$$N=b_{j,k}^0=(I_{k,j}^0/\beta_j^0)(d\chi/dU)=dI_j(2\theta)/d(2\theta) \tag{66}$$

M and N are a sort of proportional factors, as illustrated in Fig. 22, depending on the shape of diffraction peak.

Measuring $\Delta I_j^*(2\theta)$ at two different positions, $(2\theta_1, \phi_{k,j}^0)$ and $(2\theta_2, \phi_{k,j}^0)$, simultaneously by combining the half-circle sector technique with a twin-slits dector technique[37]; i.e.,

$$\Delta I_j^*(2\theta_1)=M_1\Delta I_{m,j}^*+N_1\Delta 2\theta_{B,j}^* \tag{67}$$

$$\Delta I_j^*(2\theta_2)=M_2\Delta I_{m,j}^*-N_2\Delta 2\theta_{B,j}^* \tag{68}$$

then, $\Delta 2\theta_{B,j}^*$ and $\Delta I_{m,j}^*$ can be determined from

$$\Delta 2\theta_{B,j}^*=\frac{M_2\Delta I_j^*(2\theta_1)-M_1\Delta I_j^*(2\theta_2)}{M_1N_2+M_2N_1} \tag{69}$$

$$\Delta I_{m,j}^*=\frac{N_2\Delta I_j^*(2\theta_1)+N_1\Delta I_j^*(2\theta_2)}{M_1N_2+M_2N_1} \tag{70}$$

The complex dynamic lattice strain, ε_j^* can be determined from $\Delta 2\theta_{B,j}^*$ as follows:

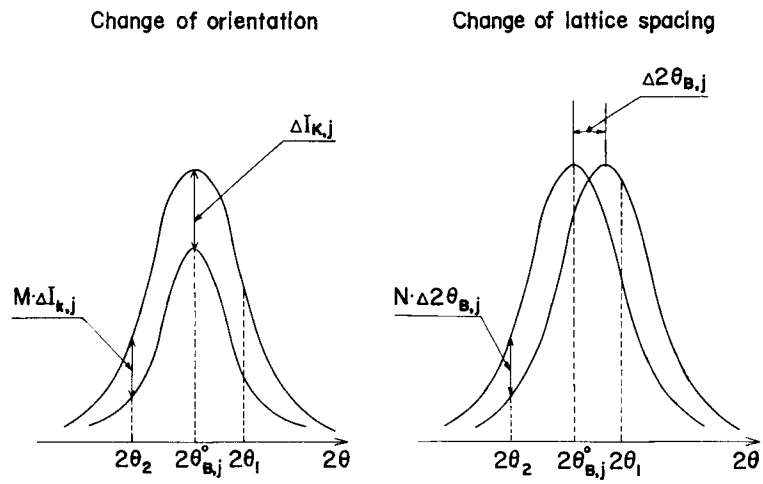

Fig. 22. Schematic diagram illustrating the change of x-ray diffraction intensity distribution from the jth crytsal planes along twice the Bragg angle at a given azimuthal angle $\phi_{k,j}^0$ due to crystal orientation (left-hand side) and lattice deformation (right-hand side). Both diagrams also illustrate the meaning of parameters, M and N.

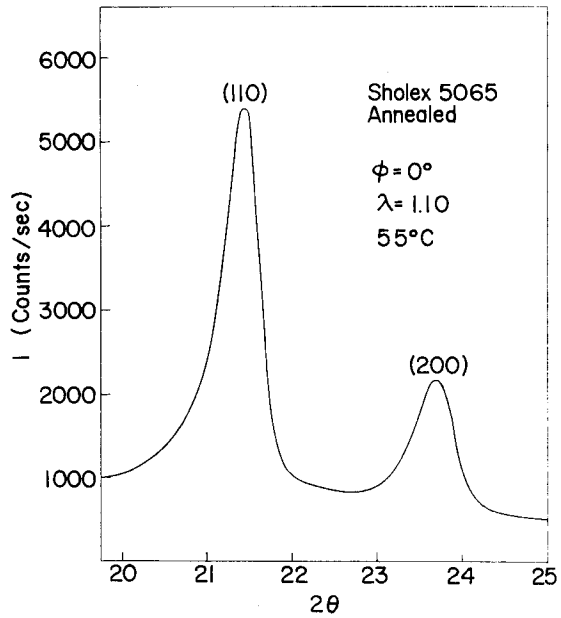

Fig. 23. Typical equatorial x-ray diffraction intensity distribution from a slightly stretched high-density polyethylene film.

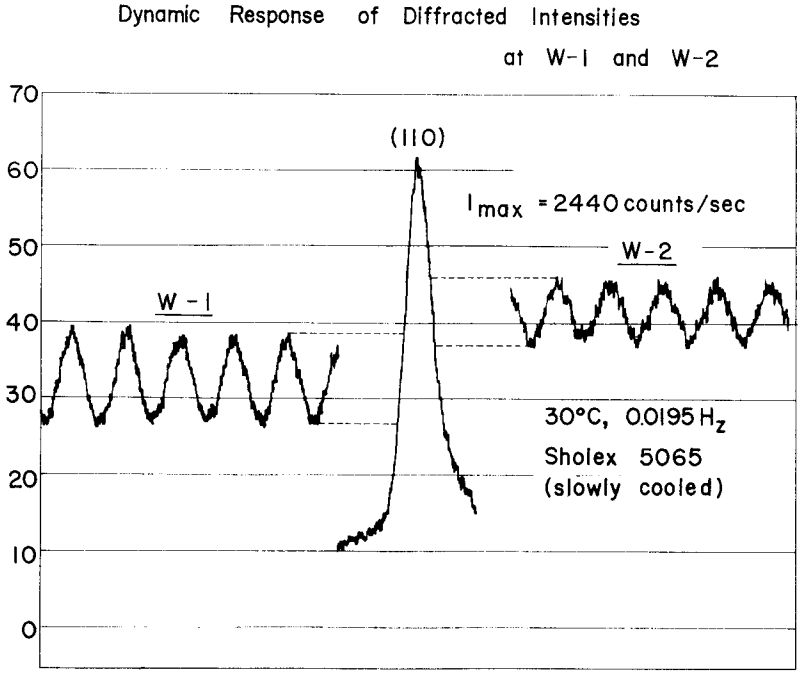

Fig. 23. Variations of x-ray diffraction intensities with sinusoidal strain of bulk specimen, which are measured by a twin-slits detector fixed at both sides of (110) diffraction peak of the annealed high-density polyethylene.

$$\varepsilon_j^* = -(1/2)\cot\theta_{B,j}{}^0 \Delta\theta_{B,j}^* \tag{71}$$

Figure 23 shows an equatorial X-ray diffraction intensity distribution from a high-density polyethylene, Sholex 5065, cast from melt at 170°C and slowly cooled down to room temperature to have a bulk density of 0.958. As seen in the figure, the (110) and (200) crystalline peaks are considerably sharp and separate from each other. These peaks, especially the (110) peak, seem to be adequate for performing the measurement of dynamic response in terms of the procedure mentioned above.

Figure 24 demonstrates the variations of X-ray diffraction intensities with sinusoidal strain, which are measured by the twin-slits dector fixed at both sides of the (110) diffraction peak, $(2\theta_1, \phi_{k,110}=0)$ and $(2\theta_2, \phi_{k,110}=0)$, for the annealed high-density polyethylene under the following static and dynamic mechanical conditions: a dynamic tensile strain of 1% superposed on a static tensile strain of 10%, vibrational frequency of 0.019 Hz, and measuring temperature of 30°C. As seen in the figure, the variations of the diffracted intensities are quite detectable and also sinusoidal, from which $\Delta I_j^*(2\theta_1)$ and $\Delta I_j^*(2\theta_2)$ can be determined by using the half-circle sector technique.

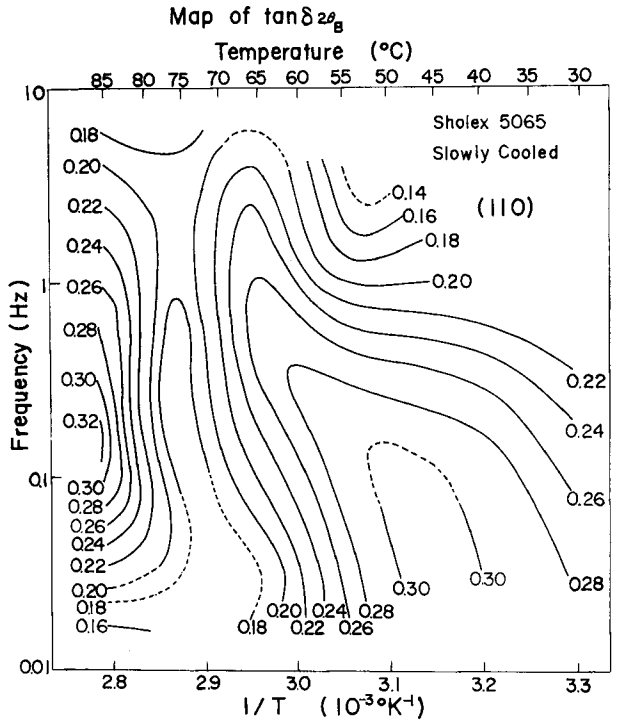

Fig. 25. Frequency and temperature dependences of tan δ_1, tangent of the phase difference between the lattice deformation and bulk strain for the (110) crystal plane of the annealed high-density polyethylene.

Figure 25 shows the frequency and temperature dependences of $\tan\delta_1$, the phase difference between the lattice deformation and bulk strain for the (110) crystal plane of the annealed high-density polyethylene, which are measured under a geometical arrangement of the test specimen, as shown in Fig. 26, against the X-ray optical coordinates. From Fig. 25, it must be noted that the value of $\tan\delta_1$ is always positive;* i.e., the lattice deformation occurs in advance of the bulk strain, and that there exist two trails of $\tan\delta_{1,max}$ in the contour map, which are very similar with those of mechanical loss tangent of polyethylene, and definitely correspond to the so-called α_1 and α_2 relaxation processes of the material.

The existence of two types of crystalline relaxation mechanisms was first investigated in a quantitative manner by Nakayasu et al.[38] for melt-crystallized linear polyethylene, designated mechanism I and II having activation energies of 28 and 46 Kcal/mole, respectively. Since then, multiple types of crystalline relaxation mechanisms have been extensively studied by many authors,[33,39-47] mostly in terms of the so-called "relaxation maps" from experimental sources of isochronal data of dynamic modulus functions of several kinds of crystalline polymers in bulk-crystallized as well as solution grown states.

The speculated assignments for the crystalline relaxation mechanisms seem to be classified into two categories. One is a mechanism associated with the crystal disordering transition or pre-melting, and the other with the grain boundary phenomena arising from various types of crystal orientation or deformation in an amorphous

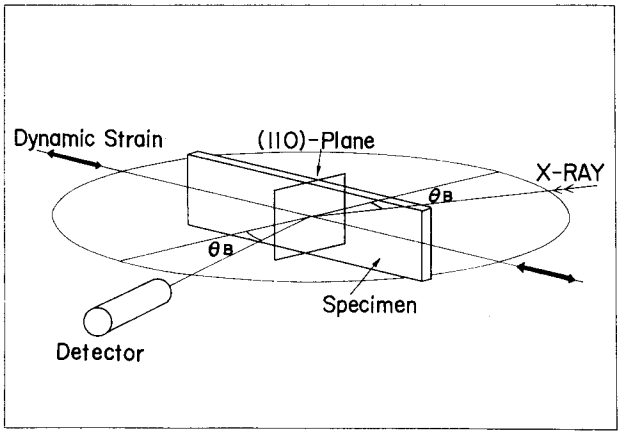

Fig. 26. Geometrical arrangement of the test specimen against x-ray optical coordinates used for obtaining the results in Fig. 25.

* As seen in Eq.(7), $2\theta_{B,j}$ is also defined as being behind the dynamic strain λ, but the observed value of δ_1 is always negative, so that $\tan\delta_1$ must be positive.

medium.[48]

Takayanagi has proposed two types of crystalline relaxation mechanisms, designated as β_c and α_c mechanisms, which are associated with the crystal disordering transition due to the onset of different modes of molecular motions of polymer chains within crystal lattice, i.e., local twisting of molecular chains around their axes and translational vibration of the chain segments along the chain axis.[39,40,43] He has added recently a mechanism, designated as α_c', arising from friction between mosaic blocks within annealed polymer crystals,[33] which may be classified as one of the grain boundary phenomena. The activation energies of β_c, α_c', and α_c mechanisms for linear polyethylene, for example, have been found as 16, 25, and 42 Kcal/mole, respectively.

On the other hand, Iwayanagi has proposed two types of crystalline relaxation mechanisms, designated as α_1 and α_2, which are associated with grain boundary phenomena of deformation and/or rotation of crystallites within a viscous medium (the amorphous phase), and with the crystal disordering transition due to the onset of torsional oscillation of polymer chains within the crystal lattice, respectively.[45] The activation energy of the α_1 mechanism is, therefore, expected to be the same order as that of the primary relaxation mechanism (β relaxation), whereas the activation energy of the α_2 mechanism for polyethylene, for example, is expected from theoretical[49,50] and experimental (NMR and dielectric)[51,52,34,35,47] sources to be several tens Kcal/mole.

Strictly speaking, however, the above assignments for the so-called crystalline relaxation processes have been based on considerable speculations, except for relatively definite, though still indirect, evidences for the α_2 process. The results of rheo-optical investigations of the dynamic orientation and lattice deformation in the previous and present sections, respectively, as well as the dynamic light scattering from spherulitic polyethylene[26,51] are the most definite evidences confirming that the so-called crystalline relaxation processes are really related to the crystalline responses.

As mentioned previously, the spherulite deformation, which is almost instantaneous, is associated with the following two mechanisms, inter- and intra-lamellar motions of crystals: the twisting of crystal lamellae around their lamellar axis(b-axes), the rotation of mosaic blocks of the lamella mostly around their a-axis, and the tilting of molecular axes within the lamellae or mosaic blocks.[30,31] The former mechanisms appear primarily at temperatures lower than the crystal disordering temperature with an activation energy of around 25 Kcal/mole, as indicated in the previous section as well as in the previous paper,[3] whereas the latter appears at temperatures higher than the crystal disordering temperature with an activation energy of the order of 50 Kcal/mole, as also indicated in the previous section. The former mechanisms must be assigned as the α_1, the grain boundary phenomena, arising from the deformation and rotation

of (*elastic*) crystalline lamellae or mosaic blocks within the (*viscous*) medium of the amorphous phase. The latter mechanism must correspond to the α_2 mechanism arising from the deformation of (*plasto-visco-elastic*) crystal lamellae or mosaic blocks associated with the pre-melting or crystal disordering transition due to the onset of torsional oscillation of polymer chains within the crystal lattice. Whether the polymer crystals are really elastic and plasto-visco-elastic below and above the crystal disordering temperature, respectively, or not, is still a problem to be approved. This may be done by examining carefully the $\tan\sigma_j$ and $\tan\delta_{j,1}$, the phase differences of crystal orientation and lattice deformation with respect to the bulk strain, respectively, in terms of their magnitude and sign as well. This is now being carried out in the laboratory of the present authors in Kyoto.

Acknowledgements

The authors are indebted to the Toyo Rayon Science Foundation, Japan (Kenkyu Josei-kin, 1964), which enabled them to construct the dynamic X-ray diffractometer. They are grateful for the grants from the Scientific Research Fund, the Ministry of Education Japan (Kagaku Kenkyu-hi, No. 93114, 1963), and the Petroleum Research Fund of the American Chemical Society (ACS-PRF-1437-D, 1963), which enabled them to perform preliminary experiments for designing the dynamic X-ray diffractometer.

Appreciation is also expressed for the financial support provided by the grants from the Japan Synthetic Rubber Co., Ltd., Tokyo, Japan, and the Bridgestone Tire Co., Ltd., Tokyo, Japan, which enables them to carry out their research work on the dynamic orientation crystallization of rubberlike materials.

References

1) R. S. Stein,: J. Polymer Sci., *C***15**, 185 (1966).
2) H. Kawai, T. Ito, D. A. Keedy, and R. S. Stein: J. Polymer Sci., B**2**, 1075 (1964).
3) T. Kawaguchi, T. Ito, H. Kawai, D. A. Keedy, and R. S. Stein: Macromolecules, **1**, 126 (1968).
4) T. Ito, T. Oda, H. Kawai, T. Kawaguchi, D. A. Keedy, and R. S. Stein: Rev. Sci. Instr., **39**, 1847 (1968).
5) T. Oda and R. S. Stein: J. Polymer Sci., B, **9**, 543 (1971); J. Polymer Sci., A-2, **10**, 685 (1972).
6) M. F. Acken and W. E. Singer: Ind. Eng. Chem., **24**, 54 (1932).
7) J. D. Long and W. E. Singer: Ind. Eng. Chem., **26**, 543 (1934).
8) D. J. Dunning and P. J. Pennells: Rubber Chem. Technol., **41**, 1381 (1968).
9) H. Kawai, T. Oda, S. Tomita, and I. Furuta: Proc. 5th Intern. Cong. Rheology, **4**, 51 (1970).
10) S. Nomura, H. Kawai, I. Kimura, and M. Kagiyama: J. Polymer Sic., A-2, **8**, 383 (1970).
11) H. Hiratsuka and S. Suehiro M.S. theses presented to the Department of Polymer Chemistry, Faculty of Engineering, Kyoto University, March 9 and 10, 1971.
12) H. Hiratsuka, M. Hashiyama, S. Tomita, and H. Kawai, paper presented at the U. S.-Japan Joint Seminor on Polymer Solid State, Cleveland, Oct. 9, 1972; J. Macromolecular Sci.-Phys., in press.

13) E. H. Andrews, Proc. Royal Soc., *A***270**, 232 (1963).
14) E. H. Andrews, Proc. Royal Soc., A**277**, 562 (1964).
15) A. Tanaka, E. P. Chang, B. Delf, I. Kimura, and R. S. Stein, submitted to J. Polymer Sci., A-2.
16) H. Leaderman, Elasticity and Creep Properties of Filamentous Materials, the Textile Foundation Inc., Washington, D. C., 1943; R. S. Marvin, E. R. Fitzgerald, and J. D. Ferry, J. Appl. Phys., **21**, 197 (1950); F. Schwarzl and A. J. Staverman, J. Appl. Phys., **23**, 838 (1952).
17) J. D. Ferry, J. Am. Chem. Soc., **72**, 3746 (1950).
18) Z. W. Wilchinsky, J. Appl. Phys., **30**, 792 (1959); **31**, 1969 (1960).
19) O. Kratky, Kolloid-Z., **84**, 149 (1938).
20) See, for example, P. H. Geil, Polymer Single Crystals, J. Wiley, New York (1963).
21) I. L. Hay and A. Keller, Kolloid-Z., **204**, 43 (1965).
22) K. Kobayashi and T. Nagasawa, J. Polymer Sci., *C***15**, 163 (1966).
23) P. Erhardt and R. S. Stein, J. Polymer Sci., B**3**, 553 (1965).
24) P. Erhardt and R. S. Stein, J. Appl. Polymer Sci., Applied Polymer Symposia, No. 5, 113 (1967).
25) R. S. Stein, Polymer Engineering and Science, **9**, 320 (1969).
26) T. Hashimoto, Static and Dynamic Light Scattering Study of Crystalline Polymer Films, Ph. D. Thesis, University of Massachusetts, 1970.
27) K. Sasaguri, R. Yamada, and R. S. Stein, J. Appl. Phys., **35**, 3188 (1964).
28) J. J. van Aartsen and R. S. Stein, J. Polymer Sci., A2, **9**, 295 (1971).
29) T. Oda, S. Nomura, and H. Kawai, J. Polymer Sci., A**3**, 1993 (1965); T. Oda, N. Sakaguchi, and H. Kawai, J. Polymer Sci., *C***15**, 223 (1966).
30) H. Kawai, Proc. 5th Intern. Cong. Rheology, **1**, 97 (1969).
31) S. Nomura, A. Asanuma, S. Suehiro, and H. Kawai, J. Polymer Sci., A-2, **9**, 1991 (1971).
32) R. S. Stein, Polymer Eng. and Sci., **8**, 259 (1968); **9**, 320 (1969).
33) M. Takayanagi and T. Matsuo, J. Macromol. Sci.-Phys., *B***1**, 407 (1967).
34) C. A. F. Tujinman, Polymer, **4**, 259, 315 (1968).
35) P. J. Phillips, G.L. Wilkes, B. W. Delf and R. S. Stein, J. Polymer Sci., A-2, **9**, 499 (1971).
36) S. Suehiro, M. S. Thesis presented to the Department of Polymer Chemistry, Faculty of Engineering, Kyoto University, March 9, 1970; S. Suehiro, T. Ito, and H. Kawai, paper presented at the 18th Annual Symposium on Rheology, Japan, Odawara, Oct. 8, 1969.
37) H. Kawai, T. Ito, and S. Suehiro, Mem. Fac. Eng., Kyoto Univ., **32**, 416 (1970).
39) M. Takayanagi, Proc. 4th Intern. Cong. Rheol., **1**, 161 (1965),.
40) M. Takayanagi, S. Minami, K. Neki, and A. Nagai, J. Soc. Materials Sci., Japan, **14**, 343 (1965).
41) N. G. McCrum and E. L. Morris, Proc. Roy. Soc. (London), *A***292**, 506 (1966).
42) K. M. Sinnott, J. Appl. Phys., **37**, 3385 (1966); J. Polymer Sci., *C***14**, 141 (1966).
43) M. Takayanagi, Intern. Symposium on Macromolecular Chemistry, Tokyo and Kyoto, 1966, Butterworth, London, 1969, p. 555.
44) M. Nakatani, K. Iijima, A. Suganuma, and H. Kawai, J. Macromol. Sci. Phys., *B***2**, 55 (1968).
45) S. Iwayanagi, paper presented at the 2nd Kyoto Seminor on Polymers, Kyoto, 1968.
46) K. Tajiri, Y. Fujii, M. Aida, and H. Kawai, J. Macromol. Sci.-Phys., *B***4**, 1 (1970).
47) T. Hideshima and M. Kakizaki, paper persented at the U. S.-Japan Joint Seminor on Polymer Solid State, Cleveland, Oct. 11, 1972; J. Macromol. Sci.-Phys., in press.
48) N. Saito, K. Okano, S. Iwayanagi, and T. Hideshima, in Solid State Physics (H. Ehrenreich, F. Seitz, and D. Turnbull, eds.), Vol. 14, Acamdeic Press., New York, 1962, p. 458.
49) K. Okano, J. Polymer Sci., *C***15**, 95 (1966).
50) R. Hayakawa and Y. Wada, Rept. Progr. Polymer Phys., Japan, **9**, 193 (1966).